EUROPEAN ORGANIZATION FOR NUCLEAR RESEARCH

CERN/SPSLC 95-27
SPSC/I 204
March 28, 1995

Letter of Intent

SEMI-INCLUSIVE MUON SCATTERING FROM A POLARISED TARGET

INFN Bari and University of Bari, Italy
E. Nappi, F. Posa

University of Bielefeld, Germany
G. Baum, S. Bültmann, D. Krämer

University of California, Los Angeles, CA, USA
C. Dulya, M. Grosse Perdekamp, G. Igo, C. Whitten

University of Freiburg, Germany
H.J. Kessler, U. Landgraf, A. Witzmann

Helsinki University of Technology, Finland
P. Berglund, J. Kyynäräinen

University of Houston, TX, USA
B. Mayes, L. Pinsky

JINR, Dubna, Russia
V. Artemov, R. Drevenak, M. Finger, M. Finger Jr., N. Gagunashvili, A. Janata, S. Jaschenko, A. Karev, Yu. Kisselev, V. Krivokhijine, V. Kurbatov, K. Medved, A. Nagaitsev, D. Peshekhonov, D. Pose, I. Savin, M. Slunecka, G. Smirnov, S. Vorozhtsov

University of Mainz, Germany
D. von Harrach, E.M. Kabuß, G.K. Mallot, J. Pretz, A. Steinmetz

University of Mons-Hainaut, Belgium
R. Windmolders

Inst. for Nuclear Research, Moscow, Russia
V. Bolotov, E. Guschin, A. Proskuryakov, V. Shmatkov, V. Lebedev

Nagoya University, Japan
T. Hasegawa, N. Hayashi, N. Horikawa, S. Ishimoto, T. Iwata, A. Kishi, T. Matsuda, K. Mori

NIKHEF, FOM and Free University, Amsterdam, The Netherlands
T.J. Ketel, P.J. Mulders

Inst. for High Energy Physics, Protvino, Russia
V.Kryshkin, V. Polyakov

DAPNIA, CEN Saclay, 91191 Gif-sur-Yvette, France
A. Magnon

University of Santiago, Santiago de Compostela, Spain
B. Adeva, G. Gracia, C. Perez, M. Plo, M. Rodriguez, J. Saborido

INFN Trieste and University of Trieste, Italy
R. Birsa, F. Bradamante, A. Bressan, S. Dalla Torre, M. Giorgi, A. Kotzinian, M. Lamanna, A. Martin, A. Penzo, P. Schiavon, F. Tessarotto, A.M. Zanetti

Soltan Institute for Nuclear Studies and Warsaw University, Warsaw, Poland
K. Kurek, J. Nassalski, E. Rondio, A. Sandacz, W. Wislicki

---

contact: G.K. Mallot *email:* gkm@cernvm.cern.ch, *mail:* CERN/PPE

Abstract

A large acceptance and high luminosity measurement of identified hadrons from deep inelastic scattering of polarised muons from a polarised solid state target is proposed. The gluon polarisation $\Delta G/G$ will be determined with a precision of $\delta(\Delta G/G) = 0.15$ from the measured asymmetries of open charm production from a longitudinally polarised target. The spin dependent quark distribution functions $\Delta u_v, \Delta d_v$, $\Delta \bar{u}$ and $\Delta \bar{d}$ and their integrals will be obtained with high accuracy. The measurement of the longitudinal polarisation of Λ and $\bar{\Lambda}$, in both, target and current fragmentation regions, will test current models for the explanation of the spin content of the nucleon and measure, for the first time, the spin transfer in fragmentation. With a transversely polarised target a first measurement of the spin dependent hadron azimuthal asymmetries can be performed. These asymmetries depend on the hitherto unmeasured twist-2 distribution functions $\Delta_T q$ of transverse spin and the Collins asymmetries in fragmentation. Transverse polarisation of $\Lambda/\bar{\Lambda}$ in the current fragmentation region also depends on $\Delta_T q$ and transverse spin transfer in fragmentation. The present measurement of g_2 will also be improved. This programme could be completed in a four year measurement (assuming current SPS performance) with a proportion of three to one for the running time with longitudinally and transversely polarised targets.

Contents

1 INTRODUCTION

After the confirmation of the original EMC finding [1, 2] by more recent experiments at CERN [3, 4] and SLAC [5, 6, 7] on the proton and the neutron, it is now firmly established that the spin content of the nucleon is not entirely due to the quarks. There are competing explanations for this result. In the gluon interpretation [8, 9, 10] it is the polarised glue ΔG which lowers the contribution of the quarks to the nucleon spin, whereas in an alternative model [11] negatively polarised strange quarks are responsible. There are several ways in which a new muon-experiment can resolve these questions.

Inclusive measurements of $g_1^{\mathsf{p}}(x), g_1^{\mathsf{n}}(x)$ and $g_2(x)$ are not able to distinguish the role of the individual parton distribution functions. It is therefore mandatory to either proceed to polarised proton-proton collisions or to perform semi-inclusive lepton scattering experiments.

A first experiment with polarised protons on a polarised proton target at FNAL [12] has been completed. The result, interpreted at leading order, appears to contradict the existence of a substantial value of $\Delta G/G$ at a gluon momentum fraction $\eta \approx 0.15$. The leading polarisation dependent process, gg to two jets, however quickly looses sensitivity once $\Delta G/G$ is about 0.5, a value suggested by the most recent analysis [33]. Recently estimates of NLO effects [14] have been made, which also indicate a loss of sensitivity in this process.

At the upcoming RHIC a major programme [15] is planned to study polarised proton-proton collisions. It is foreseen to measure $\Delta G/G$ by large p_T prompt photon production. A sensitivity of $\delta(\Delta G/G) \approx 0.075$ is expected, provided higher order effects, background photons and input polarised quark distributions can be handled at an appropriate level of accuracy. The RHIC programme also comprises a measurement with transversely polarised protons, which will determine the chiral odd distribution function $h_1(x)$, also known as transversity. The polarised proton programme at RHIC will not start before the year 2000.

The programme proposed here uses the complementary approach of exploiting semi-inclusive observables in DIS. At a diagrammatic level this is equivalent to hadron-hadron collisions with the exception that cross sections depend instead of $\sigma \sim DF \otimes DF$ on $\sigma \sim DF \otimes FF$, where DF and FF denote distribution and fragmentation functions, respectively.

For the measurement of ΔG we propose to use the photon-gluon fusion process leading to open charm production (Fig. 1). This process with real or virtual photons has been discussed [16, 17], together with J/Ψ [18] production, as a clean tool to access ΔG. The main problem was to reach sufficient statistical accuracy and background rejection for these measurements with existing accelerators. In the case of J/Ψ production only large p_T production allows a straightforward interpretation.

We will also access ΔG by determining the asymmetries in the single or correlated large p_T particle production in deep inelastic scattering [10, 19, 20]. This observable will be naturally included in our measurement of hadron asymmetries in the scattering of polarised muons off a polarised target. This method has been used in the NA47 experiment of the SMC [21] to obtain the first data on $\Delta u_v, \Delta d_v$ and $\Delta \bar{u} + \Delta \bar{d}$. Similar measurements have been proposed for the HERMES experiment [22], which is being prepared at HERA. A high statistics measurement at CERN will benefit from higher beam energies (100–200 GeV) compared to HERMES ($<$ 30 GeV), since in these measurements a clean separation of current and target fragmentation as well as a good particle identification is necessary. In terms of statistics, similar accuracies will be obtained. The knowledge of spin dependent distribution functions and their integrals like $\Delta u_v, \Delta d_v$ is important, not only for future proton-proton experiments, but also for distinguishing between different models. The interest in a measurement of polarised sea distributions like $\Delta\bar{u}, \Delta\bar{d}$ and of course $\Delta\bar{s}$ is evident.

The self-analysing properties of the $\Lambda(\bar{\Lambda})$ make this particle particularly interesting for spin physics. The question of whether the spin of the strange sea quarks is really anticorrelated with the proton spin – as proposed by some models [11] – can be decided by measuring the polarisation of Λ 's from target fragmentation [23]. The use of a polarised muon beam on unpolarised targets selects reactions on protons oriented anti-parallel to the virtual photon's helicity. If strange quarks are oriented predominantly antiparallel to the proton spin, then Λ 's from target fragmentation, inheriting the strange quark spin, should carry a negative polarisation (assuming negatively polarised, positive muons). The opposite Λ polarisation is expected if the spin of the nucleon is made up by a positive gluon polarisation [23].

The observation of $\Lambda(\bar{\Lambda})$ in the current fragmentation region addresses the problem of spin dependent fragmentation functions. Using a polarised muon beam on an unpolarised target, the helicity of the struck quark is known. The measurement of the polarisation of a forward produced Λ or $\bar{\Lambda}$ directly determines the spin dependent fragmentation function. This function has close relations to the spin structure functions [24] and can also be measured in e^+e^- [25].

If these spin dependent fragmentation functions are also known for transverse spins, they can be used in DIS on a transversely polarised target to measure the probability of a quark of a given flavour to be oriented parallel or antiparallel to the spin of transversely polarised nucleons [26]. This twist-2 distribution function $h_1(x)$ is different from its longitudinal counterpart $g_1(x)$ and is – like the transverse spin dependent fragmentation function – not yet measured. The difference between g_1 and h_1 depends among other things from the role of polarised gluons [27], which do not contribute to h_1. Another method to access h_1 has been proposed by Collins [26]. He suggests to measure the (transverse) spin dependent azimuthal asymmetries of leading hadrons around the virtual photon direction. The size of these asymmetries, i.e. the transverse spin dependent fragmentation functions are not yet known, but they are probably large [26, 29] as suggested by the size of typical asymmetries in soft hadron processes. We propose to measure these transverse spin asymmetries which, due to factorisation, can determine both, the distribution function and the fragmentation function, up to a normalisation factor. The

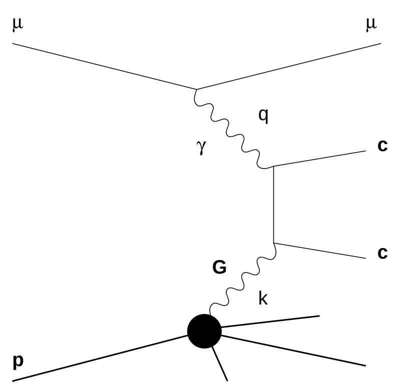

Figure 1: The photon-gluon fusion diagram.

observation of spin correlations in two jet events corresponds in the diagrammatic sense to cross sections $\sigma \sim FF \otimes FF$. There is an ongoing effort [30] to determine the transverse spin dependent fragmentation functions directly from $\mathsf{e}^+\mathsf{e}^-$.

The experimental set up to be used for the above physics programme will be built on the basis of the current SMC experiment. The measurement of hadrons however requires a few major changes and additions. The present apparatus does not use the maximum possible beam intensity due to rate limitations in the electronics and to chamber inefficiencies or instabilities in the beam region. New techniques will allow for a fivefold increase of beam intensity. (The basic EMC apparatus is now 20 years old.)

Hadron measurements compared to inclusive experiments require larger acceptance and a larger dynamical range for particle detection and identification. As already demonstrated in the NA9 [31] and E665 [32] experiments, hadron detection in this type of experiments requires a two stage magnet system. The proposed experiment will use a spectrometer magnet with 1 Tm bending power for large acceptance, and the existing forward spectrometer magnet with 4.4 Tm bending power for the small acceptance stage. Two fast RICH detectors are foreseen for particle identification, crucial for most of the programme. A special problem is posed by the polarised target which needs a homogeneous 2.5 T polarising field. The construction of a coil with about 60 cm diameter is necessary in order not to cut the hadron acceptance severely.

In summary we propose a rich spin physics programme which can be completed in a running time of four years. It will need about two years of preparation and could start in 1998. It makes use of the unique CERN muon beam which will be exploited to the limits of production target heating. Concurrent activities are limited either by duty cycle (SLAC), by beam energy (HERMES) or by nonexistence of the unique polarised target and a muon beam (FNAL). RHIC activities will start somewhat later and are be considered as complementary to the programme proposed here.

2 GLUON POLARISATION $\Delta G/G$ FROM OPEN CHARM

One of the current theoretical explanations [8, 9, 10] for the violation of the Ellis-Jaffe sum rule requires a substantial amount of polarised glue in the nucleon. Figure 2 shows three versions of the polarised gluon distribution $\Delta G(\eta)$ [33] compatible with the currently best value for $\Delta\Sigma \simeq 0.30$ which implies an integral of $\int \Delta G(\eta) d\eta \approx 2$. It appears that this quantity has a maximum around $\eta = 0.1$ where the unpolarised gluon distribution starts to drop significantly. Typical predictions are $\Delta G/G \approx 0.5$ at $\eta \approx 0.1 - 0.15$.

Among the various suggestions to measure $\Delta G/G$ [16, 17, 20, 34, 35] we consider a study of the longitudinal spin asymmetry of open charm leptoproduction as the best option for experiments at the CERN muon beam. In the following we examine the feasibility of such a measurement. We also follow the suggestion [9, 16] to use the full virtual photon spectrum, down to quasi-real photons. The proposed measurement is based on the reconstruction of D mesons from their hadronic decay products. The background due to the ordinary inelastic interactions of quasi-real photons has been carefully considered.

Heavy quarks are produced via the photon-gluon fusion process shown in Fig. 1. The cross section for muoproduction of open charm is given by

$$\frac{\mathrm{d}^2\sigma^{\mu N \to \mathsf{c}\bar{\mathsf{c}}X}}{\mathrm{d}Q^2 \mathrm{d}\nu} = \Gamma(E; Q^2, \nu)\, \sigma^{\gamma^\star N \to \mathsf{c}\bar{\mathsf{c}}X}(Q^2, \nu) \qquad (1)$$

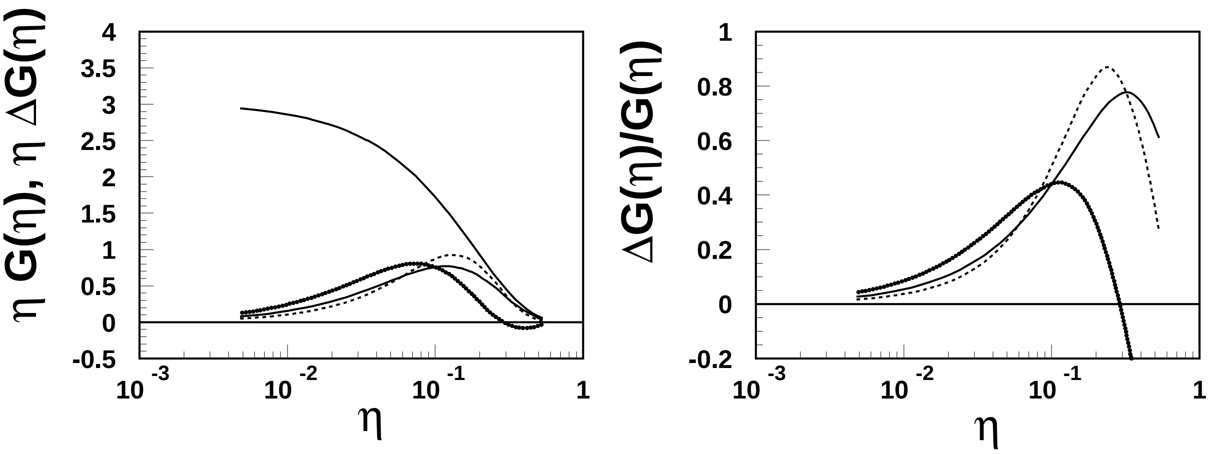

Figure 2: Three possible shapes of the polarised gluon distribution function ΔG. Sets A,B, and C refer to the notation of Ref. [33]. a) upper curve: $\eta G(\eta)$ (Duke & Owens) lower curve: $\eta\Delta G(\eta)$, set A (solid), set B (dashed), set C (thick), b) $\Delta G(\eta)/G(\eta)$: set A (solid), set B (dashed), and set C (thick).

ν GeV	σ^{cc} nb	$Q^2_{\min}$ GeV^2	$Q^2_{\max}$ GeV	$\Delta\nu \int_{Q_{\min}}^{Q_{\max}} \frac{\mathrm{d}\sigma^{\mathsf{cc}}}{\mathrm{d}Q^2\mathrm{d}\nu}\mathrm{d}Q^2$ nb	D	$\int \sigma_\gamma$ μb	$R = \frac{\int \sigma^c}{\int \sigma^\gamma}$
35–45	186	0.0029	15.0	0.543	0.470	0.184	$2.95 \cdot 10^{-3}$
45–55	234	0.0055	12.5	0.456	0.600	0.117	$3.90 \cdot 10^{-3}$
55–65	276	0.0089	10.0	0.375	0.724	0.077	$4.87 \cdot 10^{-3}$
65–75	309	0.0180	7.5	0.298	0.835	0.052	$5.73 \cdot 10^{-3}$
75–85	341	0.0353	5.0	0.229	0.923	0.033	$6.94 \cdot 10^{-3}$
35–85				1.9	$\overline{D}$=0.66	0.463	$\overline{R}$=$4.5 \cdot 10^{-3}$

Table 1: Cross sections for charm production as function of the photon energy ν.

and the virtual photon flux Γ by

$$\Gamma(E;Q^2,\nu) = \frac{\alpha_e}{2\pi}\frac{2(1-y)+y^2+Q^2/2E^2}{Q^2(Q^2+\nu^2)^{1/2}}, \tag{2}$$

where E is the muon energy and $y = \nu/E$. The virtual photon cross section for charm production, $\sigma^{\gamma^\star N\to \mathsf{c\bar{c}}X}(Q^2,\nu)$, is related to the photoproduction cross section, $\sigma^{\gamma N\to \mathsf{c\bar{c}}X}(\nu)$, by

$$\sigma^{\gamma^\star N\to \mathsf{c\bar{c}}X}(Q^2,\nu) = \frac{\sigma^{\gamma N\to \mathsf{c\bar{c}}X}(\nu)}{(1+Q^2/M^2)^2}. \tag{3}$$

The mass parameter $M = 3.9$ GeV is known from a fit to experimental data [36]. The photoproduction cross sections $\sigma^{\gamma N\to \mathsf{c\bar{c}}X}(\nu)$ were measured in several experiments (cf. Ref. [37] and references therein) and the values used for the rate estimates are listed in Tab. 1, column 2.

We propose to measure the spin dependent asymmetry A^{exp} for charm muoproduction, which is given by the number N_{cc} of charm events for parallel and antiparallel muon and target spin orientations

$$A^{\text{exp}} \;=\; \frac{N_{\mathsf{cc}}^{\uparrow\downarrow} - N_{\mathsf{cc}}^{\uparrow\uparrow}}{N_{\mathsf{cc}}^{\uparrow\downarrow} + N_{\mathsf{cc}}^{\uparrow\uparrow}} \tag{4}$$

$$= \quad P_B \cdot P_T \cdot f \cdot A^{\mathsf{cc}}_{\mu\mathsf{p}}(y), \tag{5}$$

where P_B and P_T are the beam and target polarisations and f is the fraction of polarisable nucleons in the target.

The asymmetry $A^{\mathsf{cc}}_{\mu\mathsf{p}}$ is related to the virtual photon asymmetry $A^{\mathsf{cc}}_{\gamma\mathsf{p}}$ by $A^{\mathsf{cc}}_{\mu\mathsf{p}} = D \cdot A^{\mathsf{cc}}_{\gamma\mathsf{p}}$, where the depolarisation of the virtual photon with respect to the muon is given by $D(y) \approx \{1-(1-y)^2\}/\{1+(1-y)^2\}$. The asymmetry $A^{\mathsf{cc}}_{\gamma\mathsf{p}}$ is given by the ratio of the helicity dependent and helicity averaged cross sections for charm production, $\Delta\sigma^{\gamma N \to \mathsf{c}\bar{\mathsf{c}}X}$ and $\sigma^{\gamma N \to \mathsf{c}\bar{\mathsf{c}}X}$. They can be expressed as a convolution of the elementary photon-gluon cross sections [34], $\Delta\sigma(\hat{s})$ and $\sigma(\hat{s})$,

$$\begin{aligned} \Delta\sigma(\hat{s}) &= \frac{4}{9}\frac{2\pi\alpha_e\alpha_s(\hat{s})}{\hat{s}}\left[-3\beta + \ln\frac{1+\beta}{1-\beta}\right] \\ \sigma(\hat{s}) &= \frac{4}{9}\frac{2\pi\alpha_e\alpha_s(\hat{s})}{\hat{s}}\left[-\beta(2-\beta^2) + \frac{1}{2}(3-\beta^4)\ln\frac{1+\beta}{1-\beta}\right], \end{aligned} \tag{6}$$

with the gluon distributions, ΔG and G,

$$A^{\mathsf{cc}}_{\gamma\mathsf{p}}(E,y) = \frac{\Delta\sigma^{\gamma N \to \mathsf{c}\bar{\mathsf{c}}X}}{\sigma^{\gamma N \to \mathsf{c}\bar{\mathsf{c}}X}} = \frac{\int_{4m_c^2}^{2M_NEy} \mathrm{d}\hat{s}\, \Delta\sigma(\hat{s})\, \Delta G(\eta,\hat{s})}{\int_{4m_c^2}^{2M_NEy} \mathrm{d}\hat{s}\, \sigma(\hat{s})\, G(\eta,\hat{s})}. \tag{7}$$

In Eqs. 6, $\beta = \sqrt{1-4m_c^2/\hat{s}}$ is the cm-velocity of the charm quark and $\hat{s} = (q+k)^2$ is the invariant mass of the photon-gluon system (q and k are the the photon and gluon 4-momenta and $\eta = \hat{s}/2M_NEy$ is the gluon momentum fraction). The asymmetry for transverse virtual photons is assumed to be described also by Eq. (7) [16]. As discussed in [20, 35] the spin dependent cross section $\Delta\sigma^{\gamma N \to \mathsf{c}\bar{\mathsf{c}}X}$ in Eq. 7, depending on the model chosen, is maximal for photon energies around 80 GeV and decreases for higher energies, whereas the spin averaged cross section $\sigma^{\gamma N \to \mathsf{c}\bar{\mathsf{c}}X}$ increases with energy. The muoproduction of D° mesons on an unpolarised target has already been studied by the EMC [36] by reconstruction of their hadronic decays.

In Fig. 3 the asymmetries $A^{\mathsf{cc}}_{\gamma\mathsf{p}}$ and $A^{\mathsf{cc}}_{\mu\mathsf{p}}$ calculated for the three models for ΔG from Fig. 2 are shown. According to the arguments given in [16] we assume this asymmetry to be independent of Q^2. We have chosen a lepton beam energy of 100 GeV since then the depolarisation factor D is large in the most relevant photon energy range $35 < \nu < 85$ GeV.

The fifth column of Tab. 1 shows the charm cross section (Eq.1) integrated over the full Q^2 range and a ν-bin of 10 GeV. The lower integration limit is given by $Q^2_{\min} = m^2_\mu \frac{\nu^2}{E(E-\nu)}$ and the upper one by $Q^2_{\max} = E(E-\nu)\cdot\theta_c^2$, where $\theta_c \leq 50$ mrad is the muon acceptance. The integrated cross section for charm leptoproduction in the range $35 < \nu < 85$ GeV is 1.9 nb and the average weighted depolarisation factor is $\overline{D} = 0.66$.

The quasi-real cross section $\sigma^{\gamma^* N \to X}$ can be parametrised with the inelastic real photon cross section of 100 μb and a formfactor $(1+Q^2/M^2)^{-1}$ with $M^2 = 0.31$ GeV^2 [39]. With the virtual photon flux Γ given by Eq. 2 we calculate the muon cross section shown in Tab. 1, column 7.

2.1 Reconstruction of the $\mathsf{D} \to \mathsf{K} + \pi$ decay

From the luminosity of 5.0×10^{37} cm^{-2}d^{-1} and the cross sections given in Tab. 1 we calculate the number of open charm events in the range $35 < \nu < 85$ GeV to $N^{\mathsf{cc}} \approx 94700$

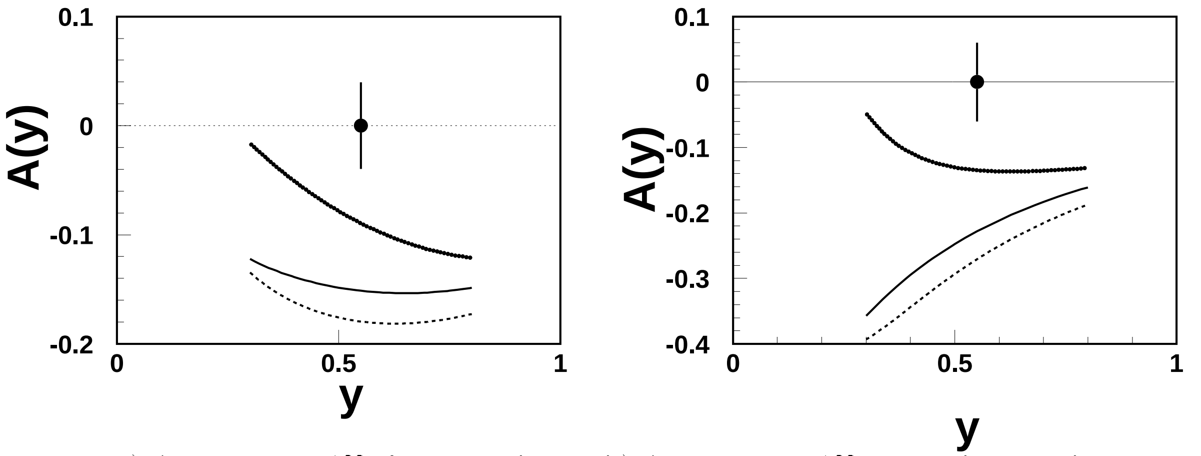

Figure 3: a) Asymmetry $A_{\mu N}^{\mathsf{cc}}$ for open charm, b) Asymmetry $A_{\gamma N}^{\mathsf{cc}}$ open charm. The curves refer like in Fig. 2 to the three sets of ΔG. The projected precision of the measurement in the range $0.35 < y < 0.85$ is indicated by the error bars of the data points shown at $A = 0$.

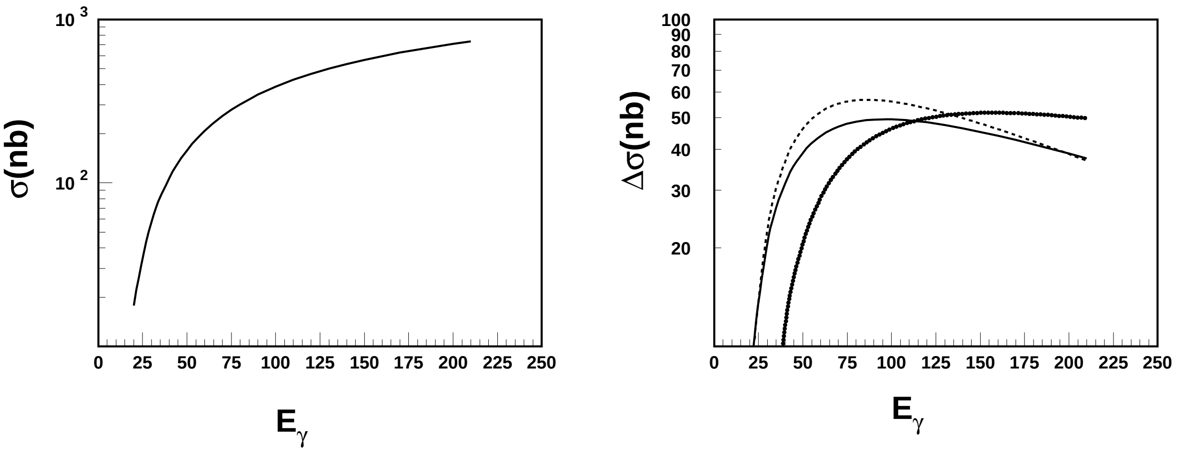

Figure 4: Charm production cross sections as a function of the photon energy $E_\gamma = \nu$. a) unpolarised cross section $\sigma^{\gamma N \to \mathsf{c}\bar{\mathsf{c}}X}$, b) polarised cross section $\Delta\sigma^{\gamma N \to \mathsf{c}\bar{\mathsf{c}}X}$.

per day. The number of non-diffractive muon events is $N^\mu \approx 23 \cdot 10^6$ per day. A proton target was assumed for these estimates.

In the following we discuss two numbers:

- $\varepsilon^{\mathsf{cc}}$, the detection probability for a charmed event and
- ε^{BG}, the number of events due to combinatorial background normalised to the number of μ-scattering events.

The detection probability $\varepsilon^{\mathsf{cc}}$ is given by the probability that a D meson was produced in a $\mathsf{c}\bar{\mathsf{c}}$ event, the branching ratio for the selected decay channel, and the acceptance a of the decay products:

$$\varepsilon^{\mathsf{cc}} = \frac{N^{\mathsf{D}}}{N^{cc}} \cdot BR \cdot a\,. \tag{8}$$

We will now concentrate on the decay $\mathsf{D}^\circ \to \mathsf{K}^- + \pi^+$ $(+C.C.)$. The acceptance, a, depends on a cut on z_D, where $z_D = E_{\mathsf{D}}/\nu$ is the energy fraction of the virtual photon energy, ν, carried by the D meson, as well as on a cut on the decay angle θ^*_{K} of the K-meson in the D's rest frame relative to the D's flight direction. Figure 5 shows the $\cos\theta^*_{\mathsf{K}}$

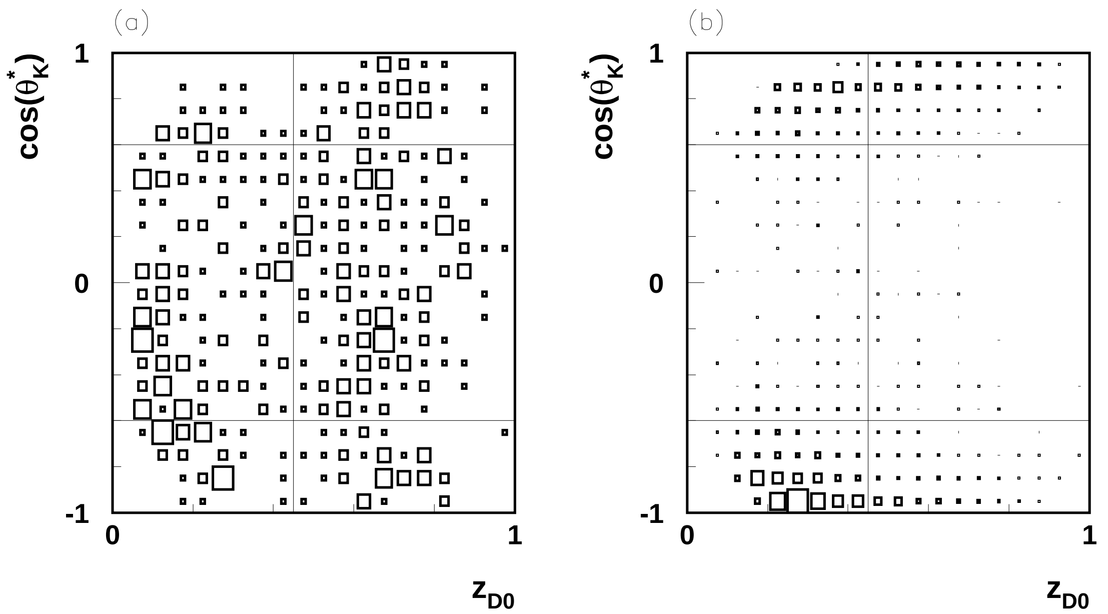

Figure 5: $\cos\theta^*_{\mathsf{K}}$ vs. z_{D}, where θ^*_{K} is the angle of the K in the CMS of the D with respect to the lab. momentum of the D (a) for K's from the decay mode $\mathsf{D} \to \mathsf{K}, \pi$ and (b) for K's from background events in a mass window of $m_{\mathsf{D}} \pm 50$ MeV. The lines indicate the cuts applied for the rate estimates.

vs. z_{D} distribution for the true D events (a) and for the background events (b) in a mass range $M_{\mathsf{D}} \pm 50$ MeV. It can be seen that the combinatorial background is concentrated at small z_{D} and θ^*_{K}. This is not surprising since ordinary fragmentation into K or π prefers low p_T and low z. The lines in the Figure indicate the cuts which were applied in order to minimise the statistical error on the D signal. Taking only D's with $z_{\mathsf{D}} > 0.45$ and $|\cos\theta^*_{\mathsf{K}}| < 0.6$ leads to an acceptance $a = 0.4$. Figure 6 shows the lab angle vs. energy distribution of the K's and the π's from the accepted D°-decays. It can be seen that particle energies are larger than ≈ 5 GeV and that an acceptance of $\theta_{\mathsf{K},\pi} < 150$–$200$ mrad is needed.

The number of $\mathsf{D}^\circ(\overline{\mathsf{D}^\circ})$ mesons per charmed event is $\frac{N^{\mathsf{D}^\circ+\overline{\mathsf{D}^\circ}}}{N^{\mathsf{cc}}}$=1.008 and the branching ratio for the selected channel $\mathsf{D}^\circ \to \mathsf{K}^-\pi^+$ is $(4.01 \pm 0.14)\%$ [38]. With these numbers we get:

$$\varepsilon^{\mathsf{cc}} = 1.008 \cdot 0.0401 \cdot 0.4 = 0.016 \tag{9}$$

The number of background events depends on the number of muon scattering events and the width of the D mass cut which has to be adapted to the mass resolution obtained in the measurement. We will use a width of $\Delta M = 40$ MeV assuming a mass resolution of $\sigma_M \approx 12$ MeV. We have determined the background reduction factor to be $\varepsilon^{\mathrm{BG}} = 1.57 \times 10^{-4}$ for $3 < Q^2 < 10$ GeV^2 and $35 < \nu < 100$ GeV. For the region $Q^2 < 3$ GeV^2 we assume the same $\varepsilon^{\mathsf{cc}}$ and $\varepsilon^{\mathrm{BG}}$. In addition we assume a shadowing reduction for $\sigma_\gamma^{\mathrm{nitrogen}}$ of $r_s = 0.9$.

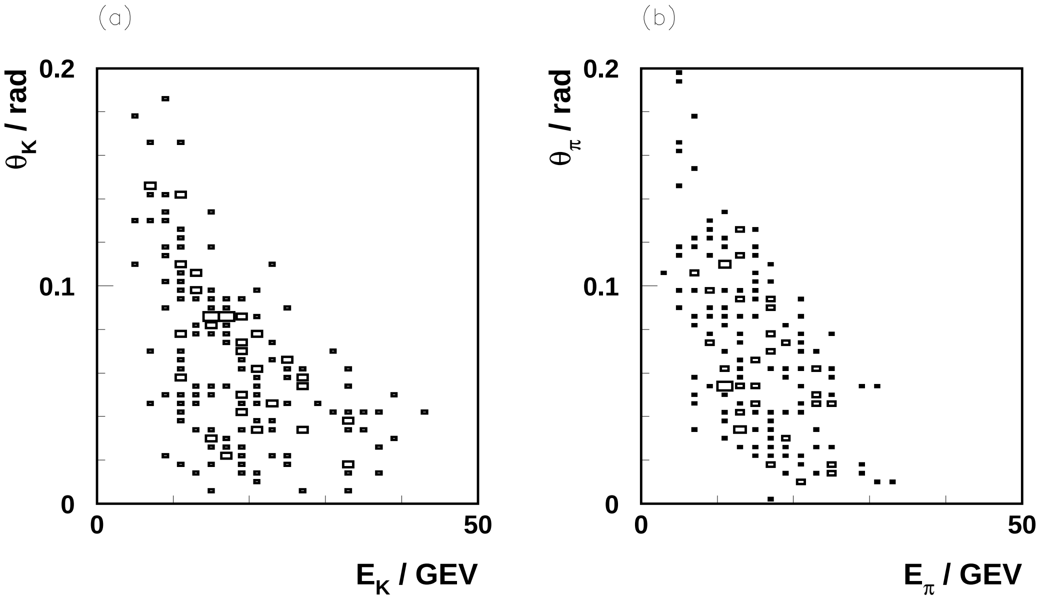

Figure 6: Energy vs. angle in the lab-system for K's (a) and π's (b) from the decay $\mathsf{D} \rightarrow \mathsf{K}, \pi$

An additional acceptance factor comes from the interaction of the $\mathsf{K}\pi$ pair with the target material. If any of the two collides, the D° is lost. For the target parameters given in Tab. 6 we obtain $\varepsilon^{\mathrm{S}}_{\mathrm{target}} = 0.71$. Also the background can be reduced if secondary interaction vertices can be detected. We have simulated secondary interaction and found that 80% of them can be rejected. We then get a reduction of the background by $\varepsilon^{\mathrm{BG}}_{\mathrm{target}} = 0.76$.

We now calculate the rate of reconstructed $\mathsf{D}^\circ, \overline{\mathsf{D}^\circ}$:

$$N^S = N^{\mathsf{cc}} \cdot \varepsilon^{\mathsf{cc}} \cdot \varepsilon^{\mathrm{S}}_{\mathrm{target}} = 1076\,\mathrm{d}^{-1} \tag{10}$$

and the background rate

$$N^{BG} = N^{\mu} \cdot \varepsilon^{BG} \cdot \varepsilon^{\mathrm{BG}}_{\mathrm{target}} \cdot r_s = 2477\,\mathrm{d}^{-1}\,. \tag{11}$$

In 112 days (3 years 25 % efficient SPS $\times$ spectrometer) the total number of events is $N^S = 120512$ and $N^{BG} = 277424$. This leads to a statistical error on the asymmetry of

$$\delta A^{\mathsf{cc}}_{\gamma\mathsf{p}} = \frac{1}{P_T P_B f \overline{D}} \frac{\sqrt{N^S + N^{BG}}}{N^S} = 0.073\,. \tag{12}$$

2.2 Recontruction of the D meson from other decay channels

There are a number of other decay channels which can be exploited to improve the statistical significance of the asymmetry, $A^{\mathsf{cc}}_{\gamma\mathsf{p}}$, e.g.

$$\begin{array}{lcll} \mathsf{D}^\circ & \rightarrow & \mathsf{K}^-\pi^+\pi^\circ & (13.8\pm1\ \ )\ \% \\ \mathsf{D}^\circ & \rightarrow & \mathsf{K}^-\pi^+\pi^+\pi^- & (\ 8.1\pm0.5\ )\ \% \\ \mathsf{D}^+ & \rightarrow & \mathsf{K}^-\pi^+\pi^+ & (\ 9.1\pm0.6)\ \%\,. \end{array}$$

We have studied these decays in some details. With cuts on z_{D} and cos θ^*_{K} we already get a substantial background reduction. Additional cuts were applied on the invariant masses of the $\mathsf{K}^-\pi^+$ and $\pi^+\pi^\circ$ sub-systems. With these cuts each of this channels leads to an error $\delta A^{\mathsf{cc}}_{\gamma\mathsf{p}} \approx 0.18$. Merging all channels brings us to an error of:

$$\delta A^{\mathsf{cc}}_{\gamma\mathsf{p}} \approx 0.06\,. \tag{13}$$

The error size is indicated in Fig. 3. The sensitivity to the polarised gluon distribution is then

$$\delta\left(\frac{\Delta G}{G}\right) \approx 0.15\,. \tag{14}$$

2.3 Comparison with other experiments on ΔG

Recent results of the fixed target experiment at Fermilab(E704) on polarised pp scattering [12] put restrictions on the size of the gluon polarisation, $\Delta G/G$, in the region $0.05 < \eta < 0.35$. It appears that large values of $\Delta G/G \approx 1$ at $\eta \approx 0.15$ can be ruled out. However, smaller values like the ones proposed more recently [33] cannot be excluded due to the quadratic dependence of the asymmetry on $\Delta G/G$. Furthermore, it appears that there are additional assumptions, like the relative contribution of various subprocesses and the neglect of NLO corrections which make the restriction on the size of $\Delta G/G$ less stringent.

The future polarised hadron experiments at RHIC consider direct photon production, pp $\rightarrow \gamma X$, as a suitable process for measuring the gluon polarisation [40]. Data can be taken at high p_T ($P_T \simeq 30$ GeV) and therefore no ambiguity in the interpretation connected with the effects of intrinsic k_T will exist. The subprocess $qg \rightarrow q\gamma$ leads to a positive contribution to A_{LL} which, in first approximation, is proportional to the product $\Delta G/G$ and $\Delta u/u$. In polarised pp collisions there are contributions to A_{LL} from different subprocesses and different Δq's which have to be known from other experiments. Background contributions from real photons, from π° decay for instance, will decrease the sensitivity. With high luminosity and high polarisations in the two beams the RHIC spin experiment expects a statistical errors in A_{LL} of 0.015 corresponding to a sensitivity $\delta\frac{\Delta G}{G} = 0.075$.

Other polarised deep inelastic lepton scattering experiments which could be considered as candidates for a measurement of the gluon polarisation are at Hera and SLAC's end station A. HERMES, with $E < 30$ GeV, has probably not enough energy [41] to investigate ΔG via the photon gluon fusion process. There have been discussions to probe $\Delta G/G$ in J/ψ production by 50 GeV real photons at SLAC, but the short duty cycle of 10^{-5} will present a formidable problem with regard to combinatorial background in the reconstruction.

3 LONGITUDINAL SPIN DISTRIBUTION FUNCTIONS

In view of the different explanations for the violation of the Ellis-Jaffe sum rule and the existence of various models for the spin structure of the nucleon it appears logical and tempting to decompose the nucleon spin into the valence and the sea components and to determine the spin distribution functions of the different flavours for the valence and the sea quarks. This can be achieved by semi-inclusive measurements of deep inelastic scattering of polarised leptons on a polarised target.

The first measurements of the semi-inclusive hadron asymmetries were performed by the EMC [2, 42], and the SMC has made the first determination of the valence, Δu_v, Δd_v

and the non-strange sea, $\Delta\overline{q}$, spin distribution functions [21]. These measurements were limited by statistics as well as by the angular acceptance of the EMC/SMC spectrometer for hadrons and the lack of particle identification. We propose here to take in parallel with the measurement of ΔG, albeit with a separate trigger, a large statistics and a large accepted sample of identified hadrons.

Estimates for the impact of such data on our knowledge of Δq_v and $\Delta\overline{q}$ are given mostly on the basis of the acceptance of the current SMC experiment scaled to the projected acceptance and luminosity of the planned experiment. Not all of the possible hadron species, e.g. K°, $\mathsf{K}^\star$, and ϕ, have yet been fully simulated.

In addition to the combination of asymmetries for the different hadrons and different targets, which is the basis for projecting out given distribution functions, we can analyse the azimuthal effects in asymmetries, the topology of the hadron jets at high $p_\perp$ and particle correlations.

For these measurements the muon energy of 100–200 GeV is of importance since it allows to get the current fragmentation functions free of target contaminants. In addition, the particle identification, necessary for the flavour and the valence-vs.-sea analysis, is easier if particles have momenta higher than 5 GeV.

3.1 Rate estimates

We assume that the event rate in the future experiment amounts to 5 times that of the SMC experiment. For a two year running with polarised targets 60 million events after analysis cuts are expected from the experience of the NA47 experiment. We further assume that the statistics is divided in 20 million events for the proton and and 40 million events for the deuteron target. The total number of accepted charged hadrons from the proton target is 35.1 M, where the shares of the different species of hadrons are 15.3 M, 13.8 M, 1.9 M and 1.9 M for π^+, π^-, K^+, and K^-, respectively. For the deuteron target these numbers are roughly twice as large. This estimate does not account for the efficiency of particle identification. On the other hand, if the NH_3 target material is used instead of butanol the statistics on protons would be higher by a factor of 1.5. The distributions of the kinematic variables x, Q^2, z, and the Feynman variable, x_F, of the events with detected hadrons are shown in Fig. 7.

The present estimate was made for muons staying in the acceptance of the FSM and causing a physics trigger. Muons too close to the beam were thus excluded from the analysis. These requirements, however, are being re-discussed for this experiment. The identification of muons which pass only through the first magnet, but not through the FSM, would double the statistics in the valence quark region of x. Recently, it has been shown [43] that using a trigger based on a the hadron calorimeter the x region can be extended down to $x = 10^{-4}$.

The hadron asymmetries are given by

$$A^h = \frac{1}{P_B P_T f D} \frac{N_h^{\uparrow\downarrow} - N_h^{\uparrow\uparrow}}{N_h^{\uparrow\downarrow} + N_h^{\uparrow\uparrow}}, \tag{15}$$

where P_B, P_T, f, and D are defined in Sec. 2, and N_h are the numbers of events for (anti)parallel orientation of muon and target spin for hadrons of type h.

The accuracy expected for the asymmetries A^{π^+}, A^{π^-}, A^{K^+}, A^{K^+}, and A^{K° for two years of running at 200 GeV are shown in Fig. 8 for the proton target and $z > 0.2$. Running at 100 GeV will not change the error bars significantly. All points are shown on

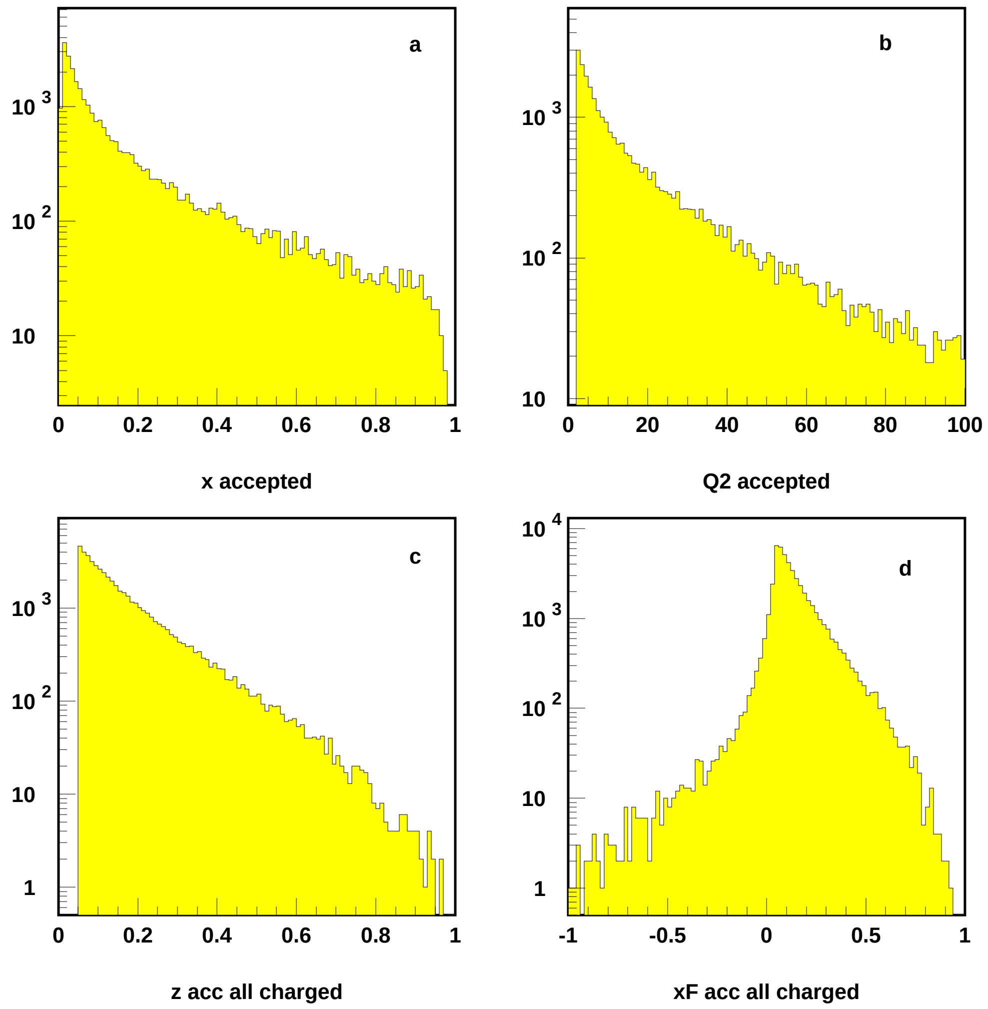

Figure 7: Distributions of (a) x, (b) Q^2, (c) z, and (d) x_F. The variables z and x_F refer to charged hadrons.

curves calculated using the Durham parametrisation of the polarised quark distribution functions [33]. Also shown are the inclusive asymmetries measured in parallel leading to errors of 0.005 and 0.004 for the proton and deuteron first moments of g_1, respectively.

3.2 Flavour decomposition of the distribution functions

The measurement and the identification of the final state hadrons in the full range of momentum allows a detailed study of the fraction of the nucleon spin carried by the valence and sea quarks, respectively. In the current fragmentation region semi-inclusive cross sections factorise into the z independent quark spin distribution functions and the x independent quark fragmentation functions. The asymmetries of the spin dependent virtual photon cross sections for muoproduction of π^+, π^-, K^+, K^-, and K° are given by the ratios of different linear combinations of quark distribution functions from which then flavour separated distribution functions can be derived as a function of x, see App. A.

The quark spin distributions determined from the asymmetries in Fig. 8 are shown

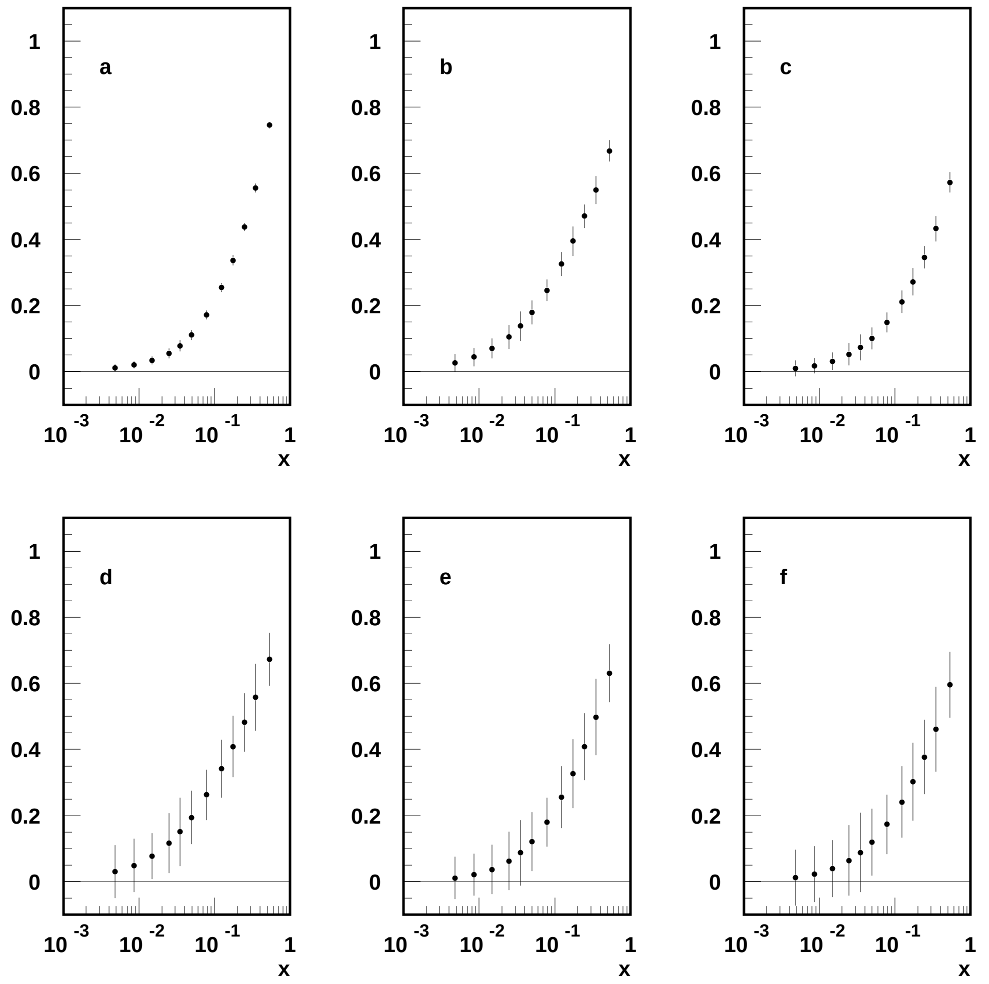

Figure 8: Inclusive asymmetry (a) and semi-inclusive asymmetries for muoproduction of (b) π^+, (c) π^-, (d) K^+, (e) K^- and (f) K° for longitudinally polarised proton target.

in Fig. 9. The integrals over x of the quark polarisations are

$$\begin{array}{rcrcl}
\int \Delta u_v \, \mathrm{d}x & = & 0.79 & \pm & 0.05, \\
\int \Delta d_v \, \mathrm{d}x & = & -0.27 & \pm & 0.07, \\
\int \Delta \overline{q} \, \mathrm{d}x & = & 0.02 & \pm & 0.03, \\
\int \Delta \overline{s} \, \mathrm{d}x & = & -0.05 & \pm & 0.10.
\end{array} \qquad (16)$$

Compared to the recent SMC results [21] the statistical errors are by a factor of five smaller for the valence quarks and by a factor of two smaller for the non-strange sea quarks, $\Delta\overline{q} = \Delta\overline{u} + \Delta\overline{d}$.

The expected statistical accuracy for the valence quark polarisation is competitive to that planed by the HERMES Collaboration [22]. The accessible x range is one order of magnitude wider and can be pushed down by almost a factor of 10 using the hadron trigger. This eliminates the source of systematic error for the integral coming from the small x extrapolation. With high statistics in the small x region a test of the the spin-

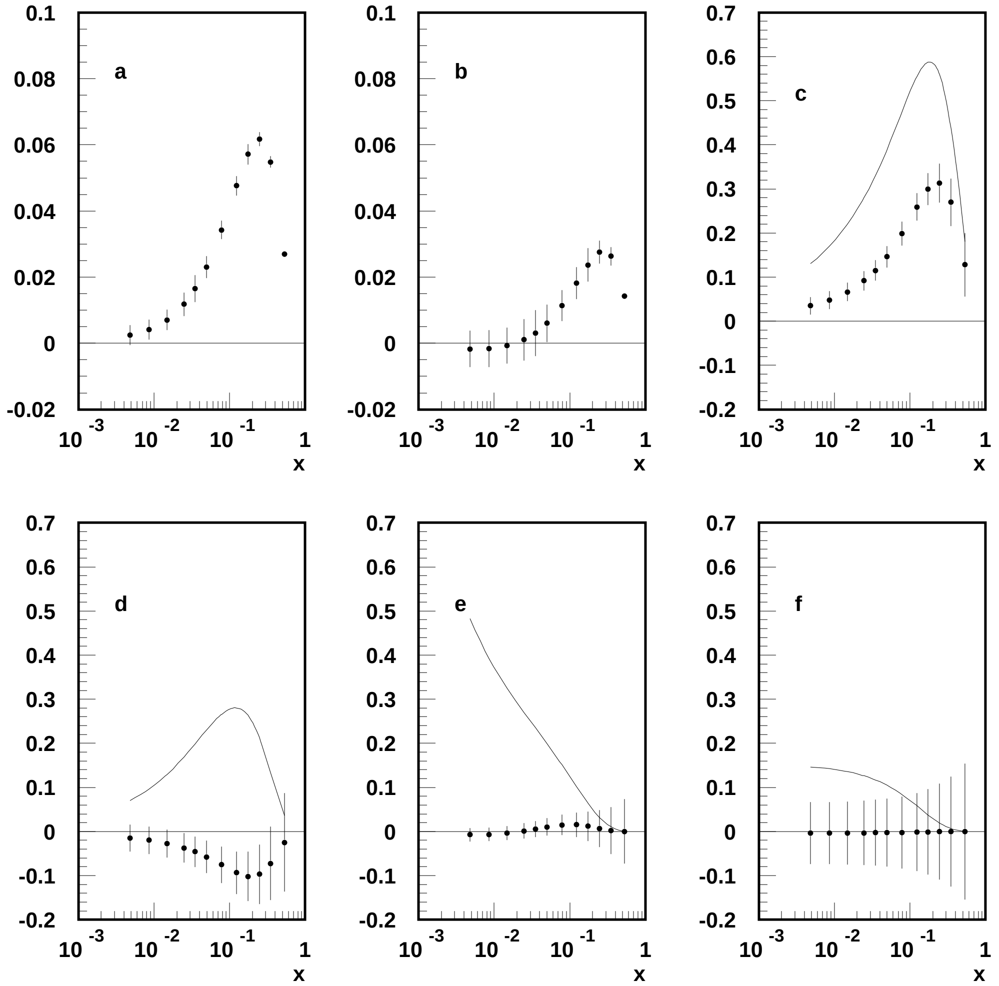

Figure 9: Spin dependent structure functions (a) xg_1^{p} and (b) xg_1^{d} and quark spin distributions (c) $x\Delta u_v$, (d) $x\Delta d_v$, (e) $x\Delta\overline{q}$ and (f) $x\Delta\overline{s}$. The solid curves represent unpolarised quark distributions.

isospin symmetry of the sea by separate determination of spin distributions of $\overline{\mathsf{u}}$ and $\overline{\mathsf{d}}$ quarks becomes feasible.

The proposed apparatus, which foresees a wide angular acceptance spectrometer close to the target gives a unique opportunity for exploratory study of semi-inclusive cross sections in the target fragmentation region. As seen in Fig. 7d a substantial fraction of hadrons with low z comes from the target fragmentation region (negative x_F). In this kinematic range the semi-inclusive cross sections do not factorise and one has to determine differential cross sections as functions of x and z simultaneously. These quantities, recently dubbed *fracture functions* [45], were proposed to be used for a study of the target (in)dependence of quark spin suppression. It is conjectured that quark polarisation is a universal feature of the axial current and not of the target structure. To examine this idea one has to measure semi-inclusive asymmetries for different final state hadrons and thus control the "target" quark contents. In particular, by selecting a final proton one probes the spin structure of the gluon-rich object with vacuum quantum numbers. The experiment is well suited for such a study because of high statistics of low z particles in the sea region of low x.

4 MEASUREMENT OF Λ AND $\overline{\Lambda}$ POLARISATION

In Sec. 2 we propose to measure the asymmetry in the production of open charm by photon-gluon fusion as a clear method to distinguish between the polarised strange quark [11] and gluon interpretation of the EMC spin effect. We will obtain complementary information on the polarisation of a struck strange quark or antiquark also by measuring the longitudinal polarisation of the Λ and $\overline{\Lambda}$ baryons.

The measurement of the Λ longitudinal polarisation in the current fragmentation region as a way to determine the spin transfer function from the struck quark to the Λ hyperon has been suggested since some time [46]. More recently it has been pointed out [23] that also the measurement of the Λ polarisation and of the Λ–$\overline{\Lambda}$ spin correlations in the target fragmentation region can help to discriminate between models with polarised strange quarks and gluons.

As discussed in section 4.2 we will access Λ's and $\overline{\Lambda}$'s produced in both, target and current fragmentation regions. While the measurement of the forward Λ's poses no particular problems, the low momentum of the decay products of the backward Λ's deserves special attention in the design of the detectors and in the analysis of the data, which needs further investigation.

4.1 The target fragmentation region

The basic idea of this measurement is that the polarised virtual photon will strike preferentially one quark polarisation state inside the target nucleon, and that the fragment left behind will contain some memory of the angular momentum removed. This may be transferred to the final state in the target fragmentation region, specifically in non-trivial longitudinal polarisation for Λ hyperons with $x_F < 0$.

Measurements of Λ polarisation in the target fragmentation region have in fact been made previously in neutrino experiments [47, 48, 49, 50]. Large negative [1)] longitudinal polarisations of the order of 0.7 was measured by WA59 [47]. The sign, the order of magnitude, and the x dependence of these data is reproduced by the polarised $\mathsf{s\bar{s}}$ model [51], which also has been used successfully to interpret data on ϕ [52] and Λ-$\overline{\Lambda}$ [53] production in proton-antiproton annihilation.

When applied to target fragmentation in deep inelastic scattering of a negatively polarised muon from a proton this model predicts large negative longitudinal polarisations of the produced Λ's and $\overline{\Lambda}$'s. More specifically the mean polarisation of a remnant s or $\bar{\mathsf{s}}$, and hence the Λ or $\overline{\Lambda}$, produced in the target fragmentation region, should be net *negative*, as shown diagrammatically shown in Fig. 10a. This is due to the preference of the virtual photon to interact with a u quark, which in average is aligned with the proton. Using this model we find negative Λ polarisations, of order -0.3 to -0.6, in the accessible range of the target fragmentation, $-0.2 < x_F < 0$. The calculation was performed for NH_3 target and standard kinematical cuts were applied. The effect is large and will be measured in this experiment, although we cannot quote errors at this stage.

It is interesting to contrast the above predictions of the polarised $\mathsf{s\bar{s}}$ sea model with the expectation for the case that the EMC/SMC spin effect is essentially due to positively

[1)] Here and in the following the sign of polarisation is given with respect to the direction of the momentum transfer, i.e. the z direction in Fig. 10

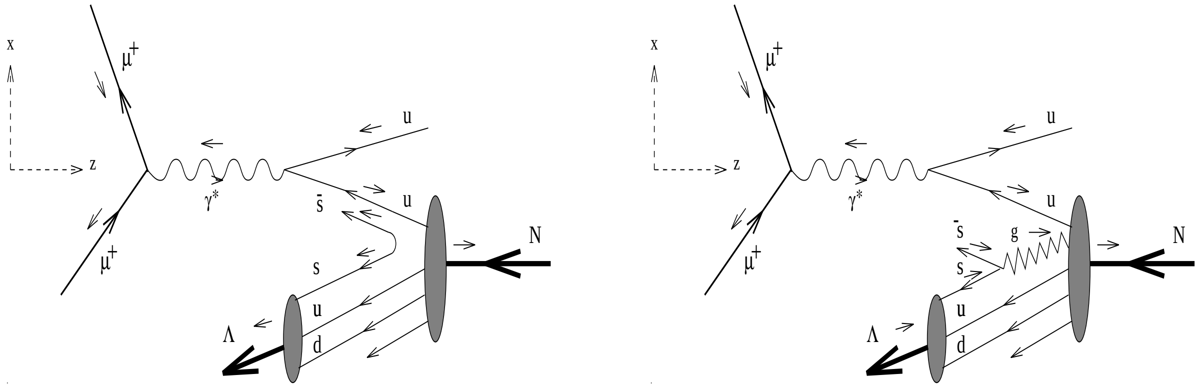

Figure 10: a) Λ polarisation according to the polarised $\mathsf{s\bar{s}}$ sea model (left) and b) in the polarised gluon model (right).

Λ's parent	$P_{\mathsf{d}} \to P_\Lambda$	$P_{\mathsf{u}} \to P_\Lambda$	$P_{\mathsf{s}} \to P_\Lambda$
Quark	0	0	+1
Σ^0	−2/9	−2/9	+1/9
$\Sigma(1385)$	+5/9	+5/9	+5/9
Ξ	−0.3	−0.3	+0.6

Table 2: Spin transfer coefficients according to BGH.

polarised gluons [8, 9, 10]. In such a model (see Fig. 10b) the Λ polarisation in the target fragmentation region is expected to be *positive*, i.e. opposite to the one for Λ's originating from a polarised $\mathsf{s\bar{s}}$ sea.

4.2 The current fragmentation region

Recently, an experimental programme to measure the polarised fragmentation function ΔD_q^Λ in $\mathsf{e^+e^-}$ has been proposed by Burkardt and Jaffe [24] (see also [54] and [55]). We propose to investigate the same quantity in semi-inclusive deep inelastic scattering of longitudinally polarised muons on unpolarised and longitudinally polarised nucleons.

In the current fragmentation region, $\Lambda/\overline{\Lambda}$'s acquire their longitudinal polarisation during polarised quark fragmentation. Its magnitude can be written as

$$P_\Lambda\,(x,y,z) = P_{\|}^{\Lambda}\,(x,y,z) = \frac{\sum_q e_q^2\,[P_B D(y) q(x) + P_T \Delta q(x)]\,\Delta D_q^\Lambda(z)}{\sum_q e_q^2\,[q(x) + P_B P_T \Delta q(x)]\,D_q^\Lambda(z)}, \tag{17}$$

where P_B and P_T denote the beam and target longitudinal polarisations, respectively, and $D(y)$ is the depolarisation factor. The observation of a non-zero $\Lambda/\overline{\Lambda}$ polarisation would be the first experimental evidence of spin transfer in polarised quark fragmentation, which can be regarded as dual to the parton distributions in polarised hadrons. For the unpolarised target case, the only unknowns in formula (17) are the polarised fragmentation functions $\Delta D_q^\Lambda(z)$.

We have studied the longitudinal Λ polarisation using the following assumptions of spin transfer mechanisms in the quark fragmentation process:

– Spin transfer according to the Bigi-Gustafson-Häkkinen [56, 57] prescription (BGH). In this approach, the Λ polarisation is described by the SU(6) non-relativistic quark model. Therefore, the polarisation of directly produced Λ's is just determined by

model	$P_d \to P_\Lambda$	$P_u \to P_\Lambda$	$P_s \to P_\Lambda$
NQM	0	0	+1
BJSR	−0.23	−0.23	+0.58

Table 3: Spin transfer coefficients according to NQM and BJSR.

that of the s-quark, while Λ's coming from other hyperon resonances also inherit part of the parent's polarisation from other quark flavours. The non-zero spin transfer coefficients we have used for this model are shown in Tab. 2.

– Spin transfer according to Burkardt-Jaffe [24]. Here, Λ's produced by strong decays of hyperon resonances are included in the Λ fragmentation function, while background of Λ's coming from Σ^0 electromagnetic decays are neglected. The reason for this, is that this channel is rather suppressed and that Λ's are depolarised by a factor 1/3 compared to the initial Σ^0's. In Tab. 3, we present the non-zero spin transfer coefficients for the naive quark model expectation (NQM) and the ones related to the the Burkardt-Jaffe sum rule (BJSR) [24], which was evaluated using the experimental value of the first moment of g_1^{p}.

For the simulation we have used the standard programs of LEPTO61 and JETSET74 [58] with their default values of parameters. We have assumed a 190 GeV μ^+ 80% negatively polarised beam focused on a two-cell proton target. The following kinematical cuts were applied:

$$\begin{array}{rcrl} Q^2 & > & 1 & \mathrm{GeV}^2/c^2 \\ y & < & 0.9 & \\ \nu & > & 20 & \mathrm{GeV} \\ p_{\mu'} & > & 20 & \mathrm{GeV}/c \\ \theta_\mu & > & 9 & \mathrm{mrad} \end{array}$$

We have generated 10^7 DIS events containing 10^6 $\Lambda/\overline{\Lambda}$ (0.8×10^6 Λ's and 0.2×10^6 $\overline{\Lambda}$'s) with charged decay modes. Assuming a spectrometer performance similar to the one of SMC in 1994 (6×10^6 μ^+ triggers) and a beam intensity five times higher, we expect around 3×10^7 μ^+-N reconstructed DIS events. In this extrapolation, we assume that the integrated cross section, reconstruction efficiency and acceptance for the scattered muon is basically the same as for SMC. In the following, all results are normalised to this number of DIS events.

In order to estimate the bias in the $\Lambda/\overline{\Lambda}$ polarisation induced by the spectrometer acceptance for proton and pion tracks, we have considered the spectrometer layout which is schematically depicted in Fig. 18. It is assumed that tracking devices with similar overall resolution and equivalent radiation lengths as SMC cover the angular acceptance defined by the two dipole magnets. The effects of resolution in the reconstructed tracks momenta have been implemented applying momentum smearing according to parametrisations based on SMC data (for a more detailed discussion of the procedure, see [59]). It was found in these first studies, that the rejection of low momentum tracks, mainly pions, due to large bending angles in the first dipole magnet limits the overall $\Lambda/\overline{\Lambda}$ acceptance.

In Fig. 11 we can see the x-Feynman distribution of both generated and accepted $\Lambda/\overline{\Lambda}$ hyperons. The geometrical acceptance of Λ tracks is around 80% in the forward region and significant losses are found only in the target fragmentation region. $\overline{\Lambda}$'s are created with larger average x_F, and their acceptance in the whole x-Feynman range is

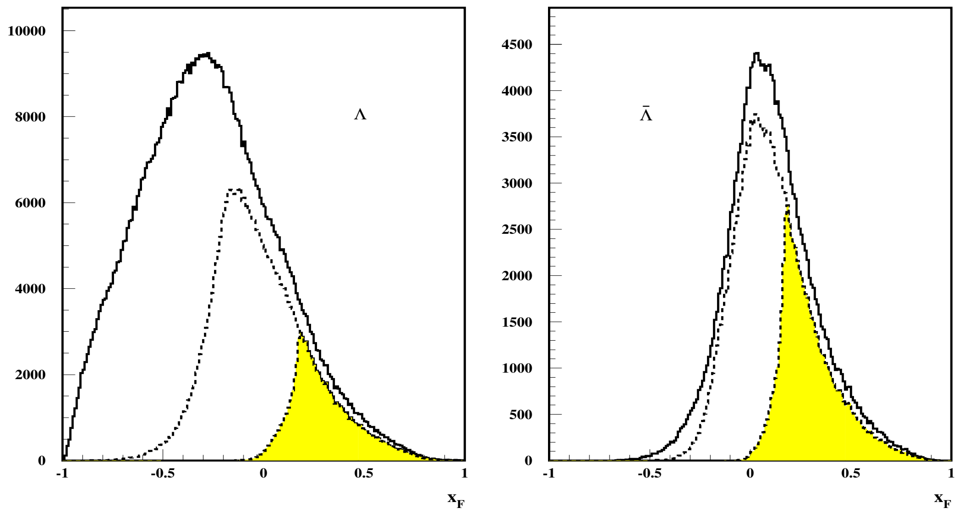

Figure 11: x-Feynman distributions of generated (solid line) and accepted (dashed) Λ (left) and $\overline{\Lambda}$ (right) samples. The hatched areas indicate the number of events that survive after the cut $z > 0.2$.

around 80%. A more detailed analysis is shown in Tab. 4.

In order to select events produced in the current fragmentation region, we applied a cut of $z > 0.2$. This means a rejection of the 70% of the reconstructable Λ's and 60% of the $\overline{\Lambda}$'s. No significative background of $\gamma \to \mathsf{e}^+\mathsf{e}^-$ and $\mathsf{K}_s^\circ \to \pi^+\pi^-$ is expected in the identification of $\Lambda/\overline{\Lambda}$ hyperons with charged decay modes thanks to the good mass resolution provided by the spectrometer and the use of the Armenteros-Podolanski method [60].

We have studied the sensitivity of the longitudinal $\Lambda/\overline{\Lambda}$ polarisation in the current fragmentation region to different mechanisms of spin transfer (those described in the previous section) for the unpolarised target nucleon case. The result is shown in Fig. 12, and it indicates a large sensitivity to ΔD_q^Λ. The difference is quite significant between the NQM and the BJSR, and might serve as an indication of "spin crisis" for Λ baryons [24].

Interval	Λ produced $(\times 10^3)$	Λ accepted $(\times 10^3)$	ratio (%)	$\overline{\Lambda}$ produced $(\times 10^3)$	$\overline{\Lambda}$ accepted $(\times 10^3)$	ratio (%)
$-1.00 < x_F < -0.60$	414	3	1	–	–	–
$-0.60 < x_F < -0.20$	1021	206	20	38	13	36
$-0.20 < x_F < +0.20$	732	590	80	397	329	83
$+0.20 < x_F < +0.60$	199	158	80	166	132	80
$+0.60 < x_F < +1.00$	20	15	74	14	10	73

Table 4: Expected number of produced and accepted $\Lambda \to \mathsf{p}\pi^-$ ($\overline{\Lambda} \to \overline{\mathsf{p}}\pi^+$) events after one year of data taking.

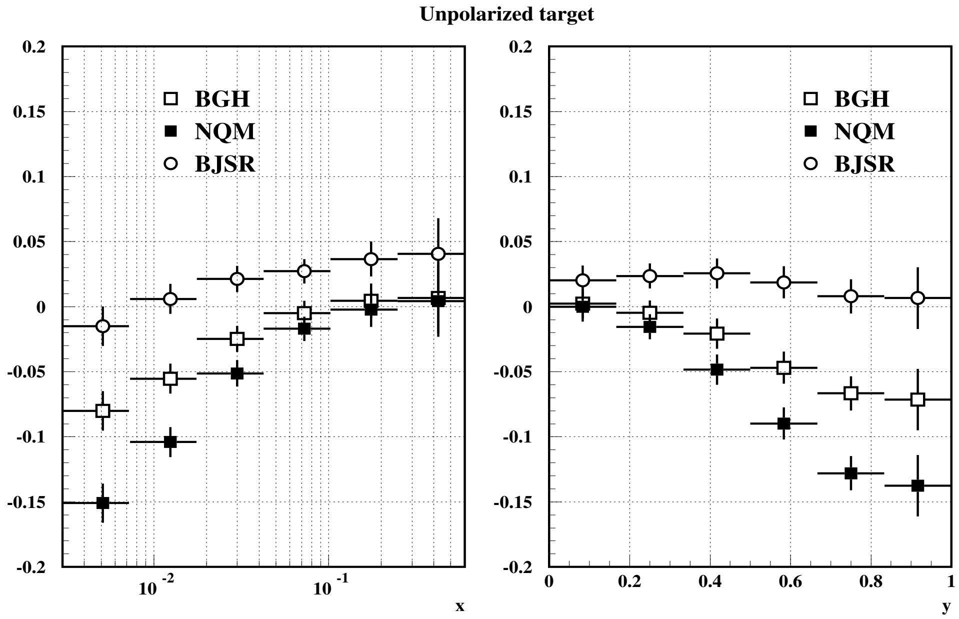

Figure 12: Λ polarisation for different mechanisms of spin transfer for the unpolarised target case.

This effect could also be enhanced by flipping the beam polarisation (μ^- beam of similar intensity).

We have observed a systematic shift in the reconstruction of the $\Lambda/\overline{\Lambda}$ polarisation towards negative values mainly caused by the rejection of low momentum tracks. This effect is important in the target fragmentation region, although it can be reduced by requiring that the Λ energy is larger than a certain threshold value. In the current fragmentation region with $z > 0.2$ the transverse polarisation of the $\Lambda/\overline{\Lambda}$ hyperons could be reconstructed without appreciable bias. Only a small shift in the longitudinal polarisation still remained (5% for initial unpolarised $\Lambda/\overline{\Lambda}$'s), but highly reduced due to the z cut. We believe that this systematic error in the polarisation reconstruction can be modeled.

5 TRANSVERSE SPIN DISTRIBUTION FUNCTIONS

We propose to measure in semi-inclusive DIS on transversely polarised proton and deuterium targets the transverse spin distribution functions $\Delta_T q(x) = q_\uparrow(x) - q_\downarrow(x)$, where $\uparrow$ ($\downarrow$) indicates a quark polarisation parallel (antiparallel) to the transverse polarisation of the nucleon. Hadron identification allows to tag the quark flavour. As shown by Jaffe and Ji [62], the momentum distributions $q(x)$, the helicity distributions $\Delta q(x)$, and the transverse spin distributions $\Delta_T q(x)$ completely specify the quark state inside the nucleon at the twist-two level.

In analogy to $g_1(x)$, it is customary [63] to construct from $\Delta_T q(x)$ a new structure function

$$h_1(x) = \frac{1}{2}\Sigma_q e_q^2[\Delta_T q(x) + \Delta_T \bar{q}(x)]. \tag{18}$$

The functions $\Delta_T q(x)$ have never been measured up to now; recently, it was proposed to measure them using the LEP beam at CERN [63] and the electron beam at HERA [22]. Complementary measurements can be done in Drell-Yan processes at RHIC [15].

Several model calculations exist for $\Delta_T q(x)$. A naive covariant *quark+scalar diquark* parton model gives $\Delta_T q(x) = \frac{1}{2}[q(x) + \Delta_L q(x)]$ [64, 27, 65]. The MIT bag model calculation [62] gives a $\Delta_T q(x)$ which has the same shape as $\Delta q(x)$ but is slightly larger. The QCD sum rule calculation of Ioffe and Khodjamirian [66] yields in the range $0.3 < x < 0.6$ a constant $\Delta_T q(x)$, which is smaller than the bag model value. In all existing estimates $\Delta_T q(x)$ is nonzero at least for u-quarks and it is different from $\Delta q(x)$.

5.1 Measurement of transversity

At variance with $g_1(x)$ which can be obtained directly from the lepton-nucleon cross-section asymmetry, $h_1(x)$ can not be measured in a single inclusive process, due to its odd chirality nature. On the other hand, $h_1(x)$ has specific signature in semi-inclusive deep inelastic scattering on transversely polarised nucleons. Since the various hadronic channels are sensitive to different quark flavours, to address the various 'pieces' of h_1 it is important to measure many different hadronic channels.

To measure $\Delta_T q(x)$ in semi-inclusive DIS, it is necessary to analyse the polarisation of the 'struck' quark. This is possible, because in the fragmentation process the leading hadron is expected to have a polarisation (or exhibit an asymmetry) related to the spin of the fragmenting quark.

Several methods will be used to measure the quark transverse polarisation. One method relies on the measurement of the transverse polarisation of Λ's ('baryon polarimeter') as proposed originally in Ref. [67], and later rediscovered by Artru and Mekhfi [27, 65]. Alternatively we will measure the azimuthal dependence of the production plane of the leading and next-to-leading hadrons [29], and the azimuthal distribution of the leading π's around the jet axis ('mesonic polarimeters') [26].

The main difficulty in all these methods is that the spin dependence of the different fragmentation functions has not yet been measured. The final hadronic asymmetries are given by the product of the polarisation of the quarks in the nucleon, the known quark spin transfer coefficient in the hard scattering and the analysing power of the fragmentation process, thus the contributions from the distribution functions (DF) and fragmentation functions (FF) to the measured asymmetry cannot be separated. Due to the factorisation of the x and z dependence in the hadronic asymmetries, the DF's $\Delta_T q(x)$ will be determined up to a normalisation constant. As suggested in Ref. [63], an absolute calibration of the analysing power of the fragmentation process should come from the analysis of two-jets events at LEP experiments.

Using the proposed experimental apparatus, all the known 'quark polarimeters' will be exploited. Here we present the method which relies on the Collins effect, i.e. on the spin dependence of the azimuthal asymmetry of the leading pion.

5.2 Collins effect for leading pions

As suggested by J. Collins [26], the fragmentation function for transversely polarised quarks should exhibit a specific azimuthal dependence. The transversely polarised quark fragmentation should be built up from two pieces, a spin-independent part, $F^0(z, P_q^{h\,2})$, and a spin-dependent part, $F^S(z, P_q^{h\,2})$:

$$F(z, \vec{P}_q^{h\,2}) = F^0(z, P_q^{h\,2}) + \frac{P_q^h}{m_F} F^S(z, P_q^{h\,2}) \sin(\phi^h - \phi^{S'}), \tag{19}$$

where m_F is a mass parameter, $\vec{P}_q^h$ is the final hadron's transverse momentum with respect to the quark direction (in our case the virtual photon direction), ϕ^h ($\phi^{S'}$) is the final

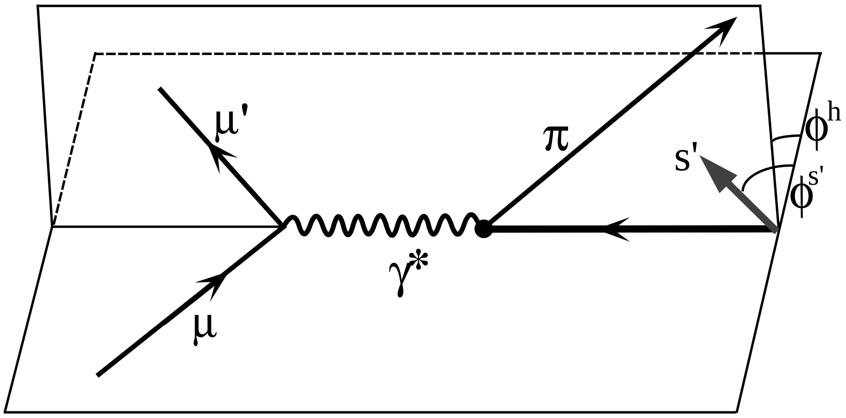

Figure 13: Definition of the Collins angle $\phi_c = \phi^h - \phi^{s'}$ in the Breit frame of the muon deep inelastic scattering.

hadron's (final quark's spin) azimuthal angle around the quark direction. In the reference frame with the z-axis along the virtual photon momentum (see fig. 13), from first order QED, the azimuthal angle of the final quark's transverse spin is given by

$$\phi^{S'} = \pi - \phi^S, \tag{20}$$

where ϕ^S is the azimuthal angle of initial quark's transverse spin. Thus, in the parton model, the transverse-spin-dependent part of the cross-section has a specific dependence on the sine of the 'Collins angle' $\phi_c = \phi^h + \phi^S$. The amplitude of this azimuthal modulation is proportional to both the transversity distribution and the analyzing power of polarised quark fragmentation.

The ratio of the polarised to the unpolarised part of fragmentation functions (the 'analyzing power') can not be calculated in perturbative QCD and up to now there is no experimental measurement. This analyzing power has been calculated in two different models: string fragmentation model [68] and low energy effective theory (linear sigma model) [26], [69]. The two approaches have shown that the effect can be very large [69]. In particular the π^+ asymmetry is expected to be large on a proton target, since DIS in this case dominantly goes with u-quark in the valence region. According to above mentioned model calculations the analyzing power can be as large as a few tenths.

The process of hadron production in DIS is more complicated when considering the intrinsic transverse momentum of the quarks inside the nucleon. In the parton model picture of Ref. [26] the spin effects connected with the transverse momentum of final hadron with respect to the scattered quark are taken into account, but the ones connected with the intrinsic transverse momentum of the initial quark in nucleon, k_T, are neglected. In the case of a polarised nucleon, the effect of k_T has recently been studied by A. Kotzinian [70] and independently by R.D. Tangerman and P.J. Mulders [71]. At the twist-2 level the quark state in a polarised nucleon is described by six distribution functions (instead of three distribution functions when k_T effects are neglected), and the semi-inclusive DIS cross section has a more complicated dependence on ϕ^S and ϕ^h. The contributions of the various distribution functions can in principle be disentangled by properly integrating on the azimuthal angles.

bin	x	ϵ	$x \cdot h_1$
1	0.006−0.04	0.0022±0.0001	0.013 ±0.001
2	0.04−0.08	0.0078±0.0003	0.037 ±0.001
3	0.08−0.10	0.0116±0.0005	0.054 ±0.003
4	0.10−0.15	0.0146±0.0004	0.065 ±0.002
5	0.15−0.20	0.0176±0.0006	0.077 ±0.003
6	0.20−0.25	0.0196±0.0009	0.081 ±0.004
7	0.25−0.30	0.0213±0.0011	0.080 ±0.004
8	0.30−0.40	0.0221±0.0012	0.071 ±0.004
9	0.40−0.50	0.0231±0.0019	0.053 ±0.005
10	0.50−1.00	0.0242±0.0028	0.028 ±0.003

Table 5: Statistical errors for the asymmetry ϵ and $x \cdot h_1(x)$ in the different x-bins, for 150 days of data taking, and $z \geq 0.1$, $E' \geq 5.$, $\nu \geq 15$.

5.3 Statistical accuracy in the measurement of $\Delta_T q$

As can be easily shown using the parton model and neglecting the intrinsic quark momentum, several combinations of the $\Delta_T q$ distribution functions can be measured, looking for the events with a leading π in DIS on transversely polarised proton and deuterium targets. A few of them are given in Appendix B. To have a first estimate of the accuracy of these measurements, we consider the asymmetry in the number of leading charged pion events on a proton target (similar considerations hold for all the proposed asymmetries).

Defining $N_p^{\uparrow} = N_p^{\pi^+\uparrow} + N_p^{\pi^-\uparrow}$ and $N_p^{\downarrow} = N_p^{\pi^+\downarrow} + N_p^{\pi^-\downarrow}$ (or $N_p^{\uparrow} = N_p^{\pi^0\uparrow}$ and $N_p^{\downarrow} = N_p^{\pi^0\downarrow}$), where the $\uparrow$ and $\downarrow$ refer to the two spin orientations of the proton, the experimental asymmetry

$$A_p = \frac{N_p^{\uparrow} - N_p^{\downarrow}}{N_p^{\uparrow} + N_p^{\downarrow}}, \tag{21}$$

can be written as

$$A_{p1} = P_T \cdot D_{nn} \cdot \frac{(4\Delta_T u + \Delta_T \bar{d} + 4\Delta_T \bar{u} + \Delta_T d)}{F_1(x)} \cdot \frac{\Delta D_u^{\pi^+} + \Delta D_u^{\pi^-}}{D_u^{\pi^+} + D_u^{\pi^-}} \cdot \sin\phi_c, \tag{22}$$

when neglecting the s quark contribution (for the notation we refer to Appendix B).

We have used a Monte Carlo program based on the LEPTO code. The events are generated in the kinematical region $0.006 \leq x \leq 1.$, at 190 Gev incident μ momentum. If the leading hadron (i.e. the most energetic particle between π's and K's) is a charged pion satisfying Berger's criterion [72] and if it has $z \geq 0.1$, an asymmetry in ϕ_c is generated according to the distribution $N(\phi_c) = N_0(1 + \epsilon \cdot \sin\phi_c)$, where:
$\epsilon = f \cdot P_T \cdot D_{nn}(y) \cdot H(x) \cdot a_c(z, P_q^h)$; f is the target polarisation dilution factor; P_T is the target polarisation; $H(x) = 2xh_1(x)/F_2(x)$; for $h_1(x)$ we have used a parametrisation [73] very closed to the one of $g_1(x)$. For a_c we have assumed the model of Ref. [68], which gives $a_c = z \cdot P_q^h \cdot \sqrt{P_q^{h\,2} + M^2}/(M^2 + P_q^h \cdot \sqrt{P_q^{h\,2} + M^2})$, with $M = 0.3$ GeV. This parametrisation gives 'reasonable' values for the asymmetry (about 0.2 at P_q^h =0.6 GeV and z =0.4).

In the analysis, only events with $\nu \geq 15$ GeV and $E' \geq 5$ GeV are accepted. The statistical errors on $x \cdot h_1$ in the 'ideal' case (π and K identification, no interaction in the target, no reconstruction errors, no large angle acceptance cut) are given in Tab. 5.3. They have been calculated assuming a luminosity of $5.8 \cdot 10^{32}$ cm$^{-2}\cdot$ s^{-1}, a 130 cm long

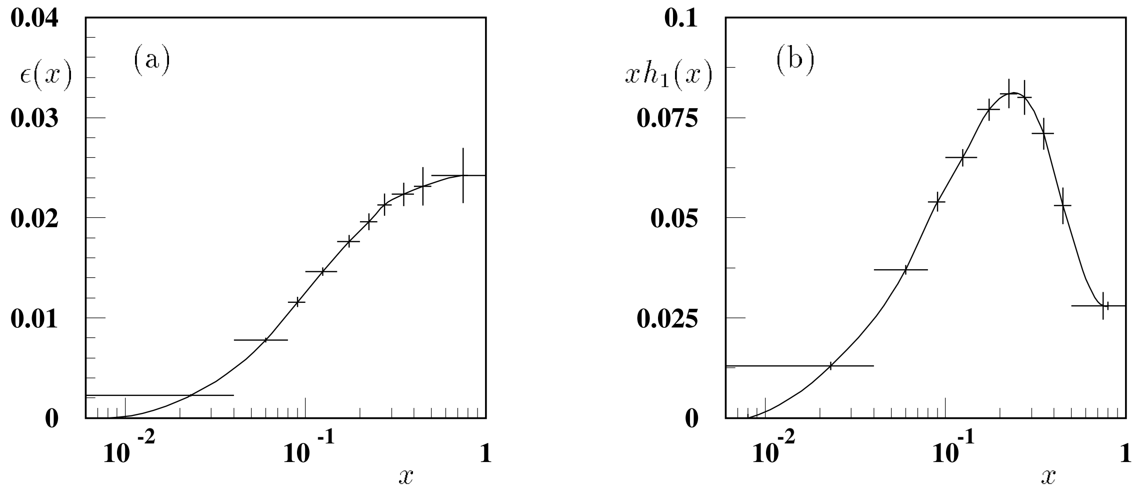

Figure 14: The expected errors on the structure function the measured asymmetry $\epsilon(x)$ (a) and $xh_1(x)$ (b) in the hypothesis of one-year of running time. The cut $z_{\rm min} = 0.1$ has been applied in selecting the leading-pion events.

NH_3 target, with a target polarisation $P_T = 85\%$, and with a dilution factor of 0.16, 150 days of data taking, and an overall efficiency of 0.25. The expected asymmetries in each x-bin are many standard deviations from zero: even if the Collins analysing power should be a factor of 5 smaller than the parametrisation we have used, it is apparent from the table that the measured ϵ would still be 2 to 7 standard deviations from zero.

Figure 14 shows the generated asymmetry in the x-range covered by the experiment, with an indication of the expected error bars (a). Also shown is the input value for the function $x \cdot h_1(x)$, as well as expected error bars (b).

5.4 Systematics uncertainties

As the particles in the jet go through the target material they interact, and it is possible that these secondary interactions introduce a dilution of the Collins asymmetry.

This effect has been studied using a Monte Carlo program based on Geant 3.21; the secondary hadronic interactions are simulated by the Gheisha package. Since by far most of the material the hadrons will go through is the target itself (each half of the present SMC target is almost one nuclear interaction length), in the simulation no other material has been considered. The SMC target consists of two cylindrical halves, each 65 cm long and 5 cm diameter. In the proposed experiment the target diameter will be 3 cm only, so the present simulation overestimates the target interactions. The deep-inelastic events are produced by the code described in the previous paragraph. The event informations are passed to the Geant-based tracking program via an external file. This file contains, for each event, the generated kinematics of the DIS event, the leading pion information (if a leading $\pi^\pm$ is present, its kinematical parameters and the Collins angle), and all the secondary-particles informations (derived from the JETSET-LEPTO event).

The effect of the secondary interactions in the target on the Collins asymmetry can be grasped in Fig. 15, where the reconstructed Collins angle ϕ_c is compared with its generated value for two categories of events, namely:

1. events where the reconstructed leading pion has the same charge of the generated leading pion (mostly “good” events);

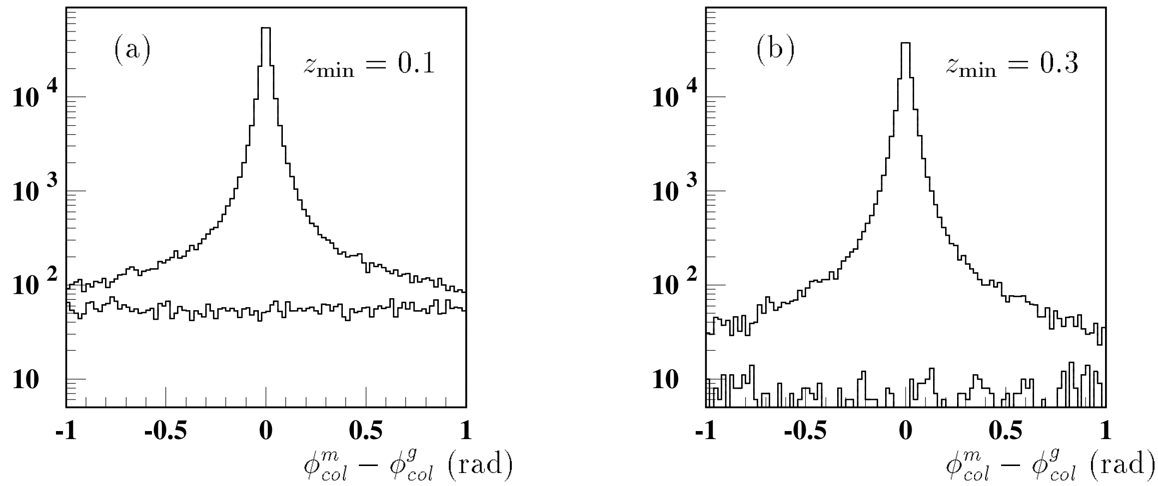

Figure 15: The difference between the measured and the generated Collins angle $\phi^m_{col} - \phi^g_{col}$ for the events with a leading π^+ in the generated event and still a π^+ after traveling through the target. The lower histogram refers to the sample $\pi^+ \to \pi^-$. (a) refers to the cut $z_{\min} = 0.1$, (b) to the cut at $z_{\min} = 0.3$.

2. events where the reconstructed leading pion has a charge opposite to the one of the generated leading pion (clearly "background" events).

It is apparent from Fig. 15 that the information on the Collins angle is completely lost for the "background" events and it is safe to assume that they show no asymmetry. It is also apparent, that most of the events in which the leading pion is not lost the Collins angle is essentially unaffected. A cut at $z_{\min} = 0.3$ allows us to reduce the "background" events by almost an order of magnitude, as suggested by the comparison of Fig. 15(a) and 15(b).

The measured asymmetry for one-year of running time is then estimated without and with the interactions in the target for the two cuts $z_{\min} = 0.1$ and $z_{\min} = 0.3$, and is shown in Fig. 16 and 17 respectively. The dilution of the asymmetry is not very large, especially for the larger $z_{\min}$ cut, it depends on the cuts, and can be estimated reliably.

To conclude, it has to be stressed that the present simulation overestimates the effect of the dilution of the asymmetry because only charged mesons are identified after the interactions in the target. The π^0 identification will help to cut down the most important source of background, namely the events with a leading π^0. Presently the π^0 is not identified and a sub-leading $\pi^\pm$ can be identified as the leading particle, and contributes to the "background", but clearly a good π^0 identification will reduce considerably this effect.

6 THE EXPERIMENTAL APPARATUS

The experiment is proposed for the M2 muon beam line. It uses part of the present NA47 spectrometer in EHN2 and the modified NA47 polarised target, and muon energies from 90 to 200 GeV. The essential differences between the requirements on the apparatus for the NA47 experiment and the new experiment are due to the high muon beam intensity of 2×10^8 muons per spill, to the need of hadron identification, and to the need of a large hadron acceptance of ± 200 mrad. Pions, kaons, and protons must be separated from 10 GeV (K/π) to 150 GeV/c, and π°'s have to be detected up 150 GeV. In the

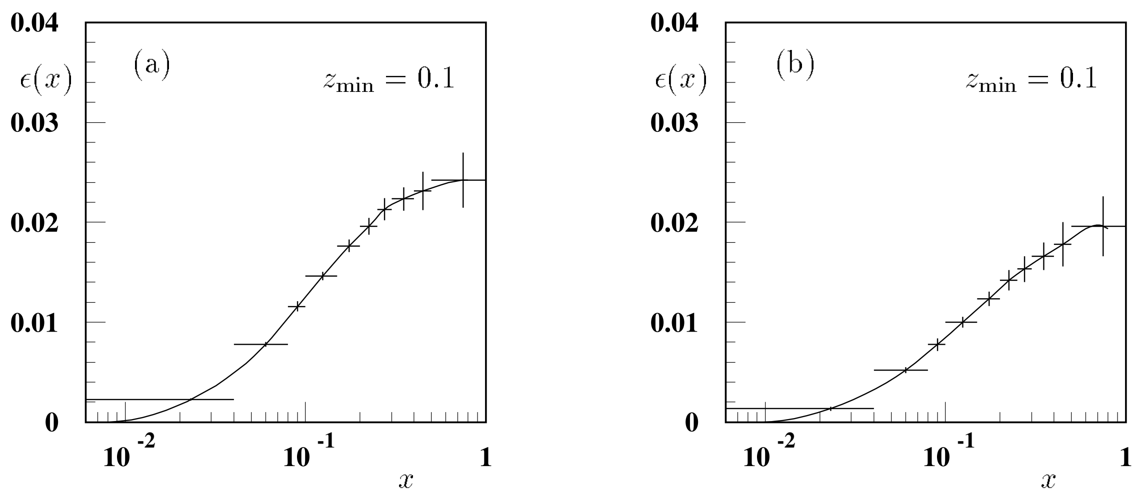

Figure 16: The measured asymmetry $\epsilon(x)$ in the hypothesis of one-year of running time, for a cut $z_{\rm min} = 0.1$. (a) shows the errors expected without target interactions; in (b) the effect of target interactions has been included.

following we concentrate on the modifications of and the additions to the present NA47 spectrometer, which are

- new beam detectors,
- an enlargement of the polarised target opening angle,
- a large aperture hadron spectrometer upstream of the present forward spectrometer magnet (FSM),
- hadron identification downstream of the FSM,
- a more selective trigger scheme, including hadron information,
- a faster data acquisition.

For the hadron identification RICH detectors and lead glass calorimeters are foreseen. Several alternatives for the new detectors are discussed below with the aim to make as much as possible use of well established techniques and to use existing devices where possible without compromising on the physics goals. The proposed spectrometer is shown schematically in Fig. 18.

6.1 Tracking considerations for the target region

The requirements on the tracking in the target region are mainly determined by the D detection in the measurement of the open charm asymmetry $A^{\mathsf{c\bar{c}}}_{\gamma \mathsf{p}}$. The D's decay within a centimetre from the lepton vertex and their re-interaction probability is negligible. But re-interactions of mesons and photons in the target material cause losses and introduce a smearing of the measured kinematical variables via multiple scattering. This also affects the determination of the D decay vertex, which has to be used to attach the event to the correct target half. The lepton vertex cannot be determined precisely for quasi-real photon interactions because the scattering angle is too small. The strategy to minimise the losses and multiple scattering without sacrificing the luminosity is a reduction of the target diameter from presently 50 to 30 mm. This must be compensated by a better focusing of the muon beam to a waist of $\sigma_x = \sigma_y = 0.8$ cm at the target. For the calculation of losses we have used the mean collision free path for meson-nucleus interactions and the mean free path of a photon for conversion to an $\mathsf{e^+e^-}$ pair.

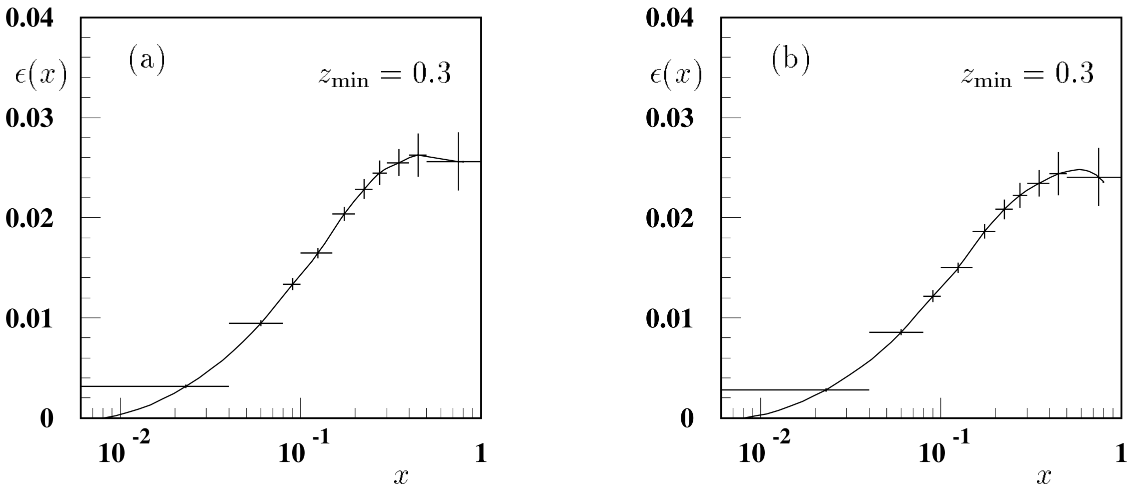

Figure 17: The measured asymmetry $\epsilon(x)$ in the hypothesis of one-year of running time and a cut $z_{\rm min} = 0.3$. (a) shows the errors expected without target interactions; in (b) the effect of target interactions has been included.

The mass resolution of the reconstructed D's has to be optimised to reduce the width of the background window (we assumed 40 MeV). From multiple scattering we expect $\delta M_{\rm D} = 8.3$, 10.8, and 13 MeV for $E_{\rm D} = 25$, 50, and 75 GeV, respectively. In order not to degrade these values any further a momentum resolution of 0.4 % at $p = 30$ GeV/c and a tracking accuracy of $\delta\theta = 70$ μrad has to be achieved.

6.2 The polarised muon beam

The planned beam intensity is 2×10^8 positive muons per spill of energies from 90 to 200 GeV. It is assumed that the present muon polarisation of about 80 % remains unchanged. The beam should be focused at the location of the polarised target with an rms width of not more than 1 cm in both, horizontal and vertical dimensions. In a test performed with L. Gatignon, SL division, in the end of the 1994 NA47 run it was shown that this beam intensity can be obtained with a proton intensity of 1.2×10^{13} per spill for a 190 GeV muon beam. For 100 GeV an about three times smaller proton intensity is sufficient.

The nominal intensity limit for the T6 production target in the M2 beam line is 10^{13} protons per spill, but this limit appears to be rather conservative and intensities of up to 40 % higher than this limit seem to be reasonable, although a careful study has to be carried out.[74]

6.3 The beam detectors

The beam detectors have to operate at a rate of about 15 MHz/cm^2 in the beam center. The rate in a 0.5 mm wide central strip will be 2 MHz. For an unambiguous correlation of the information from the beam tracking, the beam momentum measurement, and the scattered muon tracking, a time resolution of better than 1 ns is required. Tracking the muons from the location of the beam momentum measurement in the beam line tunnel to the polarised target would also establish a spatial correlation, which is presently missing.

Scintillating fibre hodoscopes combine high spatial resolution with a time resolution of better than 1 ns and a fast response of 1–2 ns, which gives them also a triggering

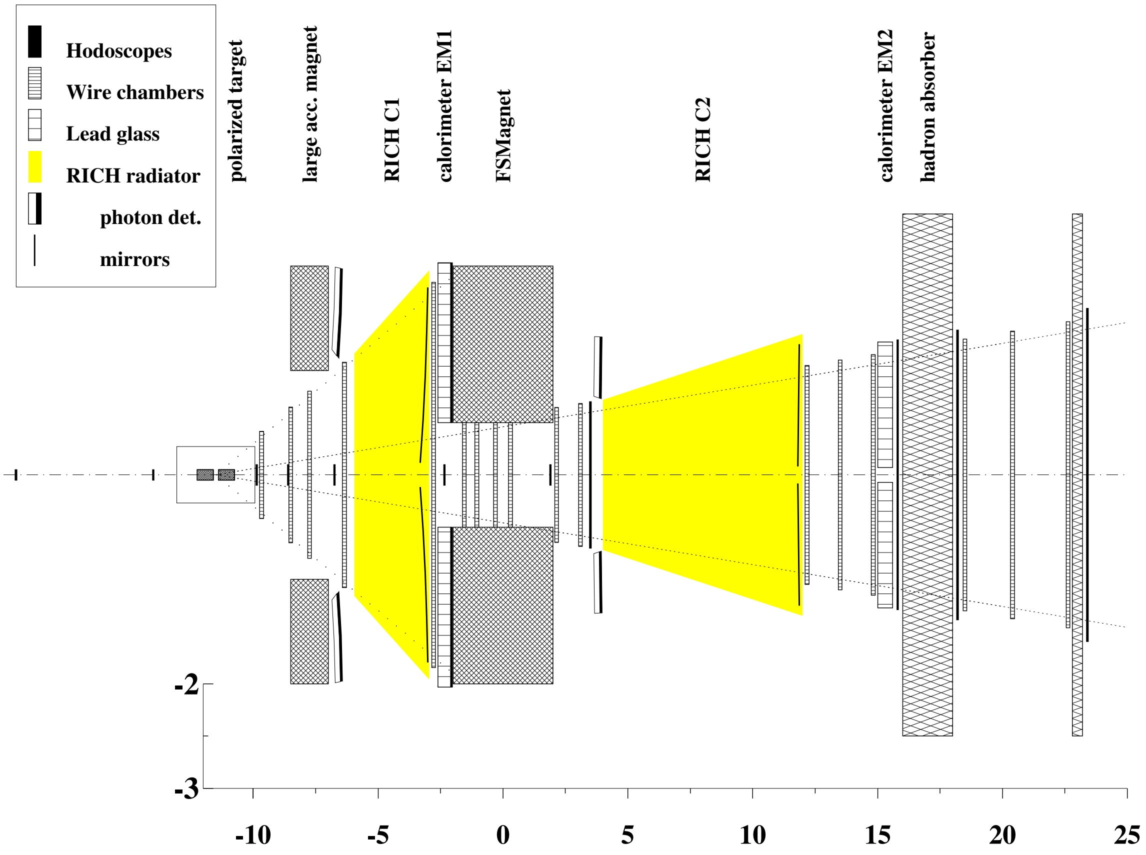

Figure 18: Proposed spectrometer for the new experiment.

Polarised target			
length of each cell		65	cm
gap between cells		25	cm
thickness (NH_3)	ρ	69	g/cm^2
dilution factor	f	0.16	
proton polarisation	P_T	0.85	
target diameter		3	cm
mean free path for K, π	λ_{coll}	99.7	g/cm^2
mean free path for $\gamma \to$ ee	λ_γ	58	g/cm^2
Muon beam			
instantaneous rate		10^8	μ/s
muons / spill		$2.0 \cdot 10^8$	
total luminosity	L	$5.0 \cdot 10^{37}$	$cm^{-2}d^{-1}$
beam polarisation	P_B	0.80	
reduction factor	$P_T P_B f \overline{D}$	0.072	
beam diameter	σ_x, σ_y	0.8	cm

Table 6: Parameters of the experiment.

capability. We propose to use hodoscopes similar to those developed in the CERN RD-17 project.[75] The prototypes consist of six layers of 0.5 mm diameter scintillating fibres. The six fibres of a 'column' are bundled onto one pixel of a position sensitive photomultiplier tube (PMT). A spatial resolution of 150 μm and detector efficiencies of close to 100 % can be achieved.

For this experiment we propose to use hodoscopes with only five layers of fibres per plane, stacked in the same way as in the RD-17 prototypes. Each hodoscopes should consist of four planes with two pairs of orthogonal fibre orientations. The material of each plane corresponds to 2.25 mm of CH_2 equivalent material, 0.5 % of a radiation length, and less than 0.3 % of an interaction length. The recently developed miniature Hamamatsu R5600 PMT has a diameter of the photocathode of only 8 mm, transition time of 0.65 ns, and a gain in excess of 10^6. It is planned to split the present one anode into four anode pads. Such a development would combine the compact packing and low costs per channel of position sensitive PMTs with the modularity and cleaner signals (no cross talk) of standard PMTs.

Altogether eight such hodoscopes would be needed, two upstream and two downstream of the polarised target, two between the hadron spectrometer magnet and the FSM, and two behind the FSM to back up the dead regions of the drift chambers. For the two most upstream hodoscopes an active area of 5×5 cm^2 corresponding to 2×400 channels is sufficient. For the other detectors a size of 12×12 cm^2 would be needed, i.e. 6×960 channels, adding up to a total of 6560 channels.

6.4 The polarised target

The materials to be used in the polarised target are ammonia for the proton target and deuterated butanol for the deuteron target. SMC proposes to prolong the NA47 experiment into 1996 using an ammonia target. If this programme is approved, all necessary technology including the measurement of the nitrogen polarisation will be available. The deuteron butanol target were used successfully by SMC in 1992 and 1994 and will also be used in the 1995 run. Polarisations of 90 % and 55 % were obtained by SMC for butanol and deuterated butanol, respectively. From the ammonia target one expects an overall gain by a factor 1.5 in the measuring time compared to butanol. Deuterated ammonia has to be irradiated *in situ* at 4 K and therefore is not feasible in the SMC polarised target.

The present superconducting solenoid of the SMC polarised target has a bore of 26 cm diameter, corresponding to an opening angle ranging from ± 65 mrad at the upstream target end over ± 100 mrad at the target center to ± 245 mrad at the downstream target end. To obtain the wanted hadron acceptance of ± 200 mrad a solenoid of 60 cm bore is needed. To design such a magnet is very challenging and alternative solutions are also being investigated.

6.5 The large angle hadron spectrometer

The hadron acceptance is presently limited also by the aperture and the big bending power of the Forward Spectrometer Magnet (FSM). It is optimised for high resolution of the scattered muon momentum.

To enlarge the hadron acceptance, the hadron detection has to be split into two sections, one upstream of the FSM for hadrons with large angles ,$>$ 40 mrad, and/or low momenta, and a section downstream of the FSM for hadrons with large momenta and angles below 40 mrad. Between the polarised target and the FSM an additional spectrometer dipole magnet with a large aperture of 2.5×2 m^2 and a pole length of

	C1	C2
Radiator gas	C_4F_{10}	CF_4/Ne
Refractive index, $n-1$	1.530×10^{-3}	0.347×10^{-3}
Maximum Čerenkov angle	55.2 mrad	26.3 mrad
Focal length, f	3.5 m	8 m
Radiator length, L	3 m	8 m
Detector response parameter, N_0	60 $\mathrm{cm^{-1}eV^{-1}}$	68 $\mathrm{cm^{-1}eV^{-1}}$
Number of detected photons, N_{ph}	55	38
Total detector efficiency	0.16	0.18
Chromatic dispersion, $\mathrm{d}n/\mathrm{d}E$	5.3×10^{-5} $\mathrm{eV^{-1}}$	6.4×10^{-6} $\mathrm{eV^{-1}}$
RICH detector constant, $\kappa_r = \sigma_\beta/\beta$	7.0×10^{-6}	1.7×10^{-6}
Photon detectors		
Detector area	2.30×0.85 m^2	1.15×1.10 m^2
Pad size	8×8 mm^2	8×8 mm^2
Number of pads	30500	19800

Table 7: Main parameters for the proposed RICH counters C1 and C2 and their photon detectors (two per RICH).

about 1.5 m will provide a field integral of about 1 Tm. The field is opposite to the one of the FSM. A design similar to the HERMES magnet [22] is presently being studied at the D.V. Efremov Scientific Research Institute of Electrophysical Apparatus in St. Petersburg, Russia, and at CERN [76]. A magnet of similar dimensions is presently in use in the NA48 experiment. Tracking partly inside the magnet will be provided by the beam detectors discussed above and proportional chambers in the outer region. Care will be taken for the fringe field, which on the upstream side must not interfere with the highly homogeneous field of the polarised target, and on the downstream side should not disturb the ring resolution of the RICH.

6.6 Particle identification

Particle identification will be performed by ring imaging Čerenkov (RICH) counters. To achieve the goal of $\pi/\mathsf{K}/\mathsf{p}$ separation in the interesting kinematic range of 10–150 GeV/c, two counters with different radiators are needed. One counter, C1, will be placed upstream of the FSM as part of the large angle hadron spectrometer and a longer counter, C2, for high particle momenta will be located downstream of the FSM. For π° detection two electromagnetic calorimeters are proposed upstream of the FSM and of the hadron absorber, respectively.

6.6.1 The RICH detectors C1 and C2

The large acceptance RICH detector, C1, is similar to the one proposed for the Hera-B experiment.[77] The length of the radiator vessel is 3 m and the transverse dimensions of the active region are 2.6×2.0 m^2 at the upstream and 4.6×3.4 m^2 at downstream end, corresponding to an angular acceptance of ± 250 mrad horizontally and ± 200 mrad vertically. The radiator gas is C_4F_{10} at atmospheric pressure and temperature. It is characterised by low dispersion and low Čerenkov threshold momenta of p_{th}= 2.6, 9.0, 17.2 GeV/c for π, K, and p, respectively. The mirror could be made by an array of about 40 hexagonal mirrors of 70 cm diameter and a focal length of 3.5 m, tilted by about

18° in the vertical plane. Thus the photon detectors can be placed away from the beam at the upper and the lower upstream ends of the RICH. We plan to use as photon detectors MWPC's with a CsI photocathode segmented in 8×8 mm^2 pads. Prototypes of such photon detectors have been built and successfully tested by the RD-26 experiment [78]. The active area of each of the two photon detectors is 2.3×0.85 m^2 and the total number of pads is 2×30500. The resolution of β, $\sigma_\beta/\beta = 7 \times 10^{-6}$, gives a 3 standard deviations π/K separation up to momenta of 70 GeV/c and a K/p separation up to 120 GeV/c. The relevant parameters are summarised together with those of RICH C2 in Tab. 7.

The design of the C2 counter downstream of the FSM is similar to the one of C1. The length of the detector is 8 m and the transverse dimensions of the active area are 2.6×1.3 m^2 upstream and 4.6×2.2 m^2 downstream. This corresponds to an angular acceptance of ± 80 mrad horizontally and ± 40 mrad vertically. The radiator gas is a mixture of CF_4 and Ne in the proportion 2:1 at atmospheric pressure and temperature. The Čerenkov threshold momenta p_{th} are 5.3, 18.7, 35.6 GeV/c for π, K, and p, respectively.

The mirrors have a focal length of 8 m and are tilted by 5° in the vertical plane. The two photon detectors are of the same type as those of the C1 detector and cover an area of 1.15×1.1 m^2 each, corresponding to 19800 cathode pads of 8×8 mm^2. The resulting resolution $\sigma_\beta/\beta = 1.7 \times 10^{-6}$ yields a three standard deviations π/K separation up to momenta of 150 GeV/c.

6.6.2 The electromagnetic calorimeters

Electromagnetic calorimeters will be placed downstream of both RICH detectors to identify π°'s in the full acceptance of the spectrometer. The upstream calorimeter EM1 should cover an area of 4×4 m^2 with a central hole of the size of the FSM aperture of 2×1 m^2. A granularity of 50×50 mm^2 is sufficient to separate the two showers for π°'s of up to 40 GeV energy. A total number of 5600 blocks of 18 radiation lengths (X_0) with a resolution of $\sigma_E/E = 7\ \%/\sqrt{E/\mathrm{GeV}}$ is assumed for this calorimeter.

The electromagnetic calorimeter EM2 in front of the hadron absorber is about 25 m downstream of the target center. To cover an angular acceptance of ± 40 mrad vertically and ± 80 mrad horizontally a size of 4×2 m^2 is needed. Neutral pions should be detected in the energy range from 30 to 150 GeV.

The GAMS lead glass calorimeter would be available for the new experiment. With a size of 2.4×2.4 m^2 it covers the central part of the acceptance. The GAMS calorimeter has a central hole of 76×76 mm^2, which nicely matches the situation at the muon beam. The inner 10×10 blocks are made of radiation-hard glass. Each block measures $38 \times 38 \times 450$ mm^3, i.e. 17 X_0. The resolution is $\sigma_E/E = 5.5\ \%/\sqrt{E/\mathrm{GeV}} + 1\ \%$. The GAMS calorimeter is fully equipped with phototubes and readout electronics.

An alternative solution is the so-called Bayan type calorimeter, a Pb/Fe-scintillator sandwich calorimeter developed at IHEP Protvino.[79] It combines good resolution with low construction costs. The scintillator strips are read out via wave length shifting fibres. A prototype has been studied using electron beams from 10–100 GeV and the GAMS NA12/2 calorimeter and a resolution of $\sigma_E/E = 5\ \%/\sqrt{E/\mathrm{GeV}} + 0.5\ \%$ was obtained. A thickness of 25 X_0 can be obtained with 80 cm long modules. For the full size of 4×2 m^2 about 4000 modules with of 45×45 mm^2 would be required.

6.7 The trigger

The present trigger in the NA47 experiment is based on horizontal and vertical hodoscopes strips. Certain allowed strip combinations provide vertical and horizontal target pointing as well as the selection of the interesting kinematic region. Such a trigger, which works in projections, is vulnerable to random coincidences, where signal from different particles simulate an interesting scattered muon. This problem will become much more severe at higher rates. Therefore we plan to use pixel hodoscopes, where the hits from different particles cannot be confused and the rates per element are much lower. A finer granularity than the present one of 10×10 cm^2 and an additional trigger hodoscope downstream of the C2 RICH will be used to improve the target pointing. The inclusion of hadron information into the trigger condition will remove radiative events as well as the in certain regions very high background from μ-escattering. In 1988 the New Muon Collaboration used a trigger requiring a certain energy deposit in a hadron calorimeter. A 3 m concrete absorber removed the hadrons downstream of this calorimeter. With this set-up a trigger efficiency of order 90 % was achieved compared to the typical value of 30 % when no hadron condition was involved. For the quasi-real photons a high resolution *energy tagger* will be constructed on the basis of scintillating fibres to detect the muons after the spectrometer magnets in the deflection plane. A muon candidate in the selected energy loss window and a hadron with a minimum z cut will provide a trigger rate of less than 4000 events per spill.

Veto rates will be in the order of 20 MHz. To avoid random vetoing, only veto signals from the elements to which the scattered muon is pointing should be applied. Depending on the beam and veto rates it could be an advantage to replace the negative veto condition by a positive beam condition.

6.8 The readout system

The readout system for this experiment will be designed with the following goals:

- it should use standard components as much as possible
- it should be able to handle events with a mean length of about 4000 16-bit words (8 kbytes)
- it should be able to handle a maximum of 10 000 events/burst
- the readout dead time for the trigger should be kept below 10 %.

The aim of 10 000 events in a burst of about 2 s together with a maximum dead time of 10 % leads to the requirement of a readout time of less than 20 μs per event. After this time the readout electronics has to be ready to accept the next event.

Using standard VME-Components a 68040 processor can perform single word (16 bit) transfers in about 200 ns/ word. Using DMA this can be improved by about a factor of 2. In the 20 μs available 100–200 words can be read. The amount of data provided by a single “equipment” (a drift chamber system, a proportional chamber system etc.) is about 100–200 words in the current NA47 experiment. Since the proposed experiment would contain about 20 such “equipments”, each of them would be read by a single VME-Processor into a local memory.

Writing to tape is another potential bottleneck: 10 000 events à 8 kbytes would produce 80 Mbytes of data/spill. In the spill pause of about 12 s, the EXABYTE 8500 drives currently used in NA47 can transfer 6 Mbytes of data (500 kbyte/s). The proposed experiment would either have to use 10 drives in parallel – this solution is for example successfully used with about 40 drives in one of the FERMILAB experiments – or one would need a faster recording device, for example the IBM 3840 compatible drives used at LEP or one of various newer tape drives that are being developed.

Although the requirements for the data acquisition are demanding, such a system can be built with presently commercially available components.

A Longitudinal spin asymmetries in hadron production

Using the parton model, and neglecting the intrinsic quark momentum, one can derive the following expressions for the hadron asymmetries

$$A_p^h = \frac{1}{P_B P_T f D} \cdot \frac{N^{\uparrow\downarrow} - N^{\uparrow\uparrow}}{N^{\uparrow\downarrow} + N^{\uparrow\uparrow}} \tag{23}$$

on a proton target, for $h = \pi+, \pi-, \mathsf{K}^+, \mathsf{K}^-$ and K^0.

$$\begin{aligned}
A_{\mathsf{p}}^{\pi^+} &= \frac{4D_1\Delta u_v + D_2\Delta d_v + 4(D_1+D_2)\Delta\bar{u} + (D_1+D_2)\Delta\bar{d} + 2D_2\Delta\bar{s}}{4D_1 u_v + D_2 d_v + 4(D_1+D_2)\bar{u} + (D_1+D_2)\bar{d} + 2D_2\bar{s}},\\
A_{\mathsf{p}}^{\pi^-} &= \frac{4D_2\Delta u_v + D_1\Delta d_v + 4(D_1+D_2)\Delta\bar{u} + (D_1+D_2)\Delta\bar{d} + 2D_2\Delta\bar{s}}{4D_2 u_v + D_1 d_v + 4(D_1+D_2)\bar{u} + (D_1+D_2)\bar{d} + 2D_2\bar{s}},\\
A_{\mathsf{p}}^{\mathsf{K}^+} &= \frac{4D_3\Delta u_v + D_4\Delta d_v + 4(D_3+D_4)\Delta\bar{u} + D_4\Delta\bar{d} + (D_3+D_4)\Delta\bar{s}}{4D_3 u_v + D_4 d_v + 4(D_3+D_4)\bar{u} + D_4\bar{d} + (D_3+D_4)\bar{s}},\\
A_{\mathsf{p}}^{\mathsf{K}^-} &= \frac{4D_4\Delta u_v + D_4\Delta d_v + 4(D_3+D_4)\Delta\bar{u} + D_4\Delta\bar{d} + (D_3+D_4)\Delta\bar{s}}{4D_4 u_v + D_4 d_v + 4(D_3+D_4)\bar{u} + D_4\bar{d} + (D_3+D_4)\bar{s}},\\
A_{\mathsf{p}}^{\mathsf{K}^0} &= \frac{8D_4\Delta u_v + (D_3+D_4)\Delta d_v + 16D_4\Delta\bar{u} + 2(D_3+D_4)\Delta\bar{d} + 2(D_3+D_4)\Delta\bar{s}}{8D_4 u_v + (D_3+D_4)d_v + 16D_4\bar{u} + 2(D_3+D_4)\bar{d} + 2(D_3+D_4)\bar{s}},
\end{aligned} \tag{24}$$

where u_v and d_v denote the valence quark distributions, $q_v = q - 2\bar{q}$.

The corresponding formulae for the deuteron are

$$\begin{aligned}
A_{\mathsf{d}}^{\pi^+} &= \frac{(4D_1+D_2)(\Delta u_v + \Delta d_v) + 5(D_1+D_2)(\Delta\bar{u} + \Delta\bar{d}) + 4D_2\Delta\bar{s}}{(4D_1+D_2)(u_v + d_v) + 5(D_1+D_2)(\bar{u} + \bar{d}) + 4D_2\bar{s}},\\
A_{\mathsf{d}}^{\pi^-} &= \frac{(D_1+4D_2)(\Delta u_v + \Delta d_v) + 5(D_1+D_2)(\Delta\bar{u} + \Delta\bar{d}) + 4D_2\Delta\bar{s}}{(D_1+4D_2)(u_v + d_v) + 5(D_1+D_2)(\bar{u} + \bar{d}) + 4D_2\bar{s}},\\
A_{\mathsf{d}}^{\mathsf{K}^+} &= \frac{(4D_3+D_4)(\Delta u_v + \Delta d_v) + 2(2D_3+3D_4)(\Delta\bar{u} + \Delta\bar{d}) + 2(D_3+D_4)\Delta\bar{s}}{(4D_3+D_4)(u_v + d_v) + 2(2D_3+3D_4)(\bar{u} + \bar{d}) + 2(D_3+D_4)\bar{s}},\\
A_{\mathsf{d}}^{\mathsf{K}^-} &= \frac{5D_4(\Delta u_v + \Delta d_v) + 2(2D_3+3D_4)(\Delta\bar{u} + \Delta\bar{d}) + 2(D_3+D_4)\Delta\bar{s}}{5D_4(u_v + d_v) + 2(2D_3+3D_4)(\bar{u} + \bar{d}) + 2(D_3+D_4)\bar{s}},\\
A_{\mathsf{d}}^{\mathsf{K}^\circ} &= \frac{(D_3+9D_4)(\Delta u_v + \Delta d_v) + (2D_3+9D_4)(\Delta\bar{u} + \Delta\bar{d}) + 4(D_3+D_4)\Delta\bar{s}}{(D_3+9D_4)(u_v + d_v) + (2D_3+9D_4)(\bar{u} + \bar{d}) + 4(D_3+D_4)\bar{s}}.
\end{aligned} \tag{25}$$

The asymmetries for the differences of cross sections for positive and negative hadrons do not depend on the fragmentation functions and are given by

$$\begin{aligned}
A_{\mathsf{p}}^{\pi^+-\pi^-} &= \frac{4\Delta u_v - \Delta d_v}{4u_v - d_v},\\
A_{\mathsf{p}}^{\mathsf{K}^+-\mathsf{K}^-} &= \frac{\Delta u_v}{u_v},\\
A_{\mathsf{d}}^{\pi^+-\pi^-} &= \frac{\Delta u_v + \Delta d_v}{u_v + d_v},\\
A_{\mathsf{d}}^{\mathsf{K}^+-\mathsf{K}^-} &= A_{\mathsf{d}}^{\pi^+-\pi^-}.
\end{aligned} \tag{26}$$

The symbols $D_{1,2,3,4}$ stand for the fragmentation functions $D_u^{\pi^+,\pi^-,\mathsf{K}^+,\mathsf{K}^-}$. The assumptions made in Eqs. 24–26 about charge conjugation and isospin symmetries were similar to those made by EMC [44].

B Transverse spin asymmetries in π production

Using the parton model, and neglecting the intrinsic quark momentum and the longitudinal polarisation of incoming lepton, here follow some combinations of the $\Delta_T q$ distribution functions which can be measured counting the number of events with a leading π in DIS on transversely polarised proton and deuterium targets:

A. With a proton target:

1. If $N_p^{\uparrow} = N_p^{\pi^+\uparrow} + N_p^{\pi^-\uparrow}$ and $N_p^{\downarrow} = N_p^{\pi^+\downarrow} + N_p^{\pi^-\downarrow}$ (or $N_p^{\uparrow} = N_p^{\pi^0\uparrow}$ and $N_p^{\downarrow} = N_p^{\pi^0\downarrow}$), where the $\uparrow$ and $\downarrow$ refer to the two spin orientations of the proton, the experimental asymmetry

$$A_{p1} = \frac{N_p^{\uparrow} - N_p^{\downarrow}}{N_p^{\uparrow} + N_p^{\downarrow}},$$

is given by:

$$A_{p1} = P_T \cdot D_{nn} \cdot \frac{(4\Delta_T u + \Delta_T \bar{d} + 4\Delta_T \bar{u} + \Delta_T d)(A_1 + A_2) + 2(\Delta_T s + \Delta_T \bar{s})A_3}{(4u + 4\bar{u} + d + \bar{d}) \cdot (D_1 + D_2) + 2(s + \bar{s}) \cdot D_3} \cdot \sin\phi_c.$$

where:
P_T = nucleon polarisation,
$D_{nn}(y) = (1-y)/(1-y+y^2/2)$ = quark spin transfer coefficient,
$D_1 = D_u^{\pi^+} = D_d^{\pi^-} = D_{\bar{u}}^{\pi^-} = D_{\bar{d}}^{\pi^+}$,
$D_2 = D_u^{\pi^-} = D_d^{\pi^+} = D_{\bar{u}}^{\pi^+} = D_{\bar{d}}^{\pi^-}$,
$D_3 = D_s^{\pi^+} = D_s^{\pi^-} = D_{\bar{s}}^{\pi^-} = D_{\bar{s}}^{\pi^+}$,
$D_{q(\bar{q})}^h(z, P_q^h) = D_{q(\bar{q})\to h}(z, P_q^h)$ = unpolarised fragmentation functions,
$\Delta_T D_{q(\bar{q})}^h(z, \vec{P}_q^h) = D_{q(\bar{q})}^{h(\uparrow)}(z, \vec{P}_q^h) - D_{q(\bar{q})}^{h(\downarrow)}(z, \vec{P}_q^h) = A_{q(\bar{q})}^h(z, P_q^h) \cdot \sin\phi_c$ = spin dependent part of the fragmentation functions,
$\Delta_T D_i = A_i \cdot \sin\phi_c$.

If we neglect the s quark (or the D_3 and A_3) contribution, we obtain:

$$A_{p1} = P_T \cdot D_{nn} \cdot \frac{(4\Delta_T u + \Delta_T \bar{d} + 4\Delta_T \bar{u} + \Delta_T d)}{F_1(x)} \cdot \frac{(A_1 + A_2)}{D_1 + D_2} \cdot \sin\phi_c.$$

2. If $N_p^{\uparrow} = N_p^{\pi^+\uparrow} - N_p^{\pi^-\uparrow}$ and $N_p^{\downarrow} = N_p^{\pi^+\downarrow} - N_p^{\pi^-\downarrow}$, the experimental asymmetry

$$A_{p2} = \frac{N_p^{\uparrow} - N_p^{\downarrow}}{N_p^{\uparrow} + N_p^{\downarrow}},$$

is given by:

$$A_{p2} = P_T \cdot D_{nn} \cdot \frac{(4\Delta_T u_v - \Delta_T d_v) \cdot (A_1 - A_2)}{(4u + 4\bar{u} + d + \bar{d}) \cdot (D_1 + D_2) + 2(s + \bar{s}) \cdot D_3} \cdot \sin\phi_c,$$

where $\Delta_T q_v = \Delta_T q - \Delta_T \bar{q}$.

If we neglect the s quark (or the D_3) contribution, we obtain:

$$A_{p2} = P_q^h \cdot D_{nn} \cdot \frac{4\Delta_T u_v - \Delta_T d_v}{F_1} \cdot \frac{A_1 - A_2}{D_1 + D_2} \cdot \sin\phi_c.$$

B. With a deuterium target:

1. If $N_d^{\uparrow} = N_d^{\pi^+\uparrow} + N_d^{\pi^-\uparrow}$ and $N_d^{\downarrow} = N_d^{\pi^+\downarrow} + N_d^{\pi^-\downarrow}$ (or $N_d^{\uparrow} = N_d^{\pi^0\uparrow}$ and $N_d^{\downarrow} = N_d^{\pi^0\downarrow}$), the experimental asymmetry

$$A_{d1} = \frac{N_d^{\uparrow} - N_d^{\downarrow}}{N_d^{\uparrow} + N_d^{\downarrow}},$$

is given by:

$$A_{d1} = P_T \cdot D_{nn} \cdot \frac{5(\Delta_T u + \Delta_T \bar{u} + \Delta_T d + \Delta_T \bar{d})(A_1 + A_2) + 4(\Delta_T s + \Delta_T \bar{s})A_3}{5(u + \bar{u} + d + \bar{d}) \cdot (D_1 + D_2) + 4(s + \bar{s}) \cdot D_3} \cdot \sin \phi_c$$

i.e. it is a different combination of the same quark distributions and fragmentation functions which appear in A_{p1}.

2. If $N_d^{\uparrow} = N_d^{\pi^+\uparrow} - N_d^{\pi^-\uparrow}$ and $N_d^{\downarrow} = N_d^{\pi^+\downarrow} - N_d^{\pi^-\downarrow}$, the experimental asymmetry

$$A_{d2} = \frac{N_d^{\uparrow} - N_d^{\downarrow}}{N_d^{\uparrow} + N_d^{\downarrow}},$$

is given by:

$$A_{d2} = P_T \cdot D_{nn} \cdot \frac{3(\Delta_T u_v + \Delta_T d_v) \cdot (A_1 - A_2)}{5(u + \bar{u} + d + \bar{d}) \cdot (D_1 + D_2) + 4(s + \bar{s}) \cdot D_3} \cdot \sin \phi_c.$$

C. Using proton and deuterium target data an other combination of quark distributions can be obtained:

$$A_{pd} = \frac{(N_d^{\pi^+\uparrow} - N_d^{\pi^-\uparrow}) - (N_d^{\pi^+\downarrow} - N_d^{\pi^-\downarrow})}{(N_p^{\pi^+\uparrow} - N_p^{\pi^-\uparrow}) - (N_p^{\pi^+\downarrow} - N_p^{\pi^-\downarrow})} = \frac{3(\Delta_T u_v + \Delta_T d_v)}{4\Delta_T u_v - \Delta_T d_v}$$

This asymmetry has an expression very similar to the one obtained in semi-inclusive DIS with longitudinally polarised targets and beam [80], and has the important feature to be independent from the value of the hadronisation analysing power.

References

[1] EMC, J. Ashman *et al.*, Phys. Lett. **B206** (1988) 364.
[2] EMC, J. Ashman *et al.*, Nucl. Phys. **B328** (1989) 1.
[3] SMC, B. Adeva *et al.*, Phys. Lett. **B302** (1993) 533.
[4] SMC, B. Adams *et al.*, Phys. Lett. **B329** (1994) 399; Phys. Lett. **B339** (1994) 332.
[5] SLAC E-142, D.L. Anthony *et al.*, Phys. Rev. Lett. **71** (1993) 959.
[6] SLAC E-143, K. Abe *et al.*, Phys. Rev. Lett. **74** (1995) 346.
[7] SLAC E-143, K. Abe *et al.*, SLAC-PUB-95-6734, *submitted to* Phys. Rev. Lett.
[8] A.V. Efremov, O. V. Teryaev, Dubna Preprint E2-88-287.
[9] G.Altarelli, G. G. Ross., Phys. Lett. **B212** (1988) 391.
[10] R.D. Carlitz, J. C. Collins, A. H. Mueller, Phys. Lett. **B214** (1988) 229.
[11] S.J. Brodsky, J. Ellis, M. Karliner, Phys. Lett. **B206** (1988) 309.
[12] D.L. Adams *et al.*, Phys. Lett. **B336** (1994) 269.
[13] T. Gehrmann and W.J. Stirling, Z. Phys. **C65** (1994) 461.
[14] M. Karliner and R.W. Robinett, Phys. Lett. **B324** (1994) 209.
[15] RHIC Spin Physics Proposal, 1992, Update Sept. 1993.
[16] M. Glück and E. Reya, Z. Phys. **C39** (1988) 569.
[17] G. Altarelli and W.J. Stirling, Particle World **Vol. 1** (1989) 40.
[18] J.Ph. Guillet, Z. Phys. **C39** (1988) 75.
[19] Fontannaz, Schiff, and Pire, Z. Phys. **C8** (1981) 349.
[20] M. Glück, E. Reya, and W. Vogelsang, Nucl. Phys. **B351** (1991) 579.
[21] SMC, W. Wislicki, Proc. XXIXth Rencontres de Moriond, Meribel, France, 1994, *QCD and High Energy Hadron Interactions*, Editions Frontieres, 1995.
[22] The HERMES Collaboration, Technical Design Report, DESY-PRC 93/06, Hamburg, 1993.
[23] J. Ellis and A. Kotzinian, CERN/TH internal note, March 1995.
[24] M. Burkardt and R.L. Jaffe, Phys. Rev. Lett. **70** (1993) 2537.
[25] F. Lamarche, talk at the *transverse Polarisation in Deep Inelastic Scattering Workshop*, Geneva, March 12–13,1993.
[26] J. Collins, Nucl. Phys. **B396** (1993) 161.
[27] X. Artru and M. Mekhfi, Z. Phys. **C45** (1990) 669.
[28] H. He and X. Ji, *preprint* MIT-CTP-2380 (1994).
[29] J. Collins, *preprint* PSU/TH/101 (1993).
[30] A. Kotzinian, private communication.
[31] EMC, Nucl. Instrum. Methods **212** (1983) 11.
[32] E665 collaboration, Nucl. Instrum. Methods **A291** (1990) 533.
[33] T. Gehrmann and W.J. Stirling, Z. Phys. **C65** (1994) 461.
[34] A.D. Watson, Z. Phys. **C12** (1982) 123.
[35] W. Vogelsang, proc. *Physics at HERA*, Hamburg, Oct. 29–30, 1991, eds. W. Buchmüller and G. Ingelman.
[36] EMC, J.J Aubert *et al.*, Phys. Lett. **167B** (1986) 127.
[37] M.P. Alvarez *et al.*, Z. Phys. **C60** (1993) 53.
[38] Particle Data Group, Phys. Rev. **D50** (1994) 1173.
[39] H. Abramowicz, E.M. Levin, A. Levy, and U. Maor, Phys. Lett. **B269** (1991) 465.
[40] G. Bunce *et al.*, Particle World **3** (1992) 1.
[41] M. Düren and K. Zapfe, *preprint* DESY 94-239, Dec. 1994.
[42] V. Papavassiliou, PhD Thesis, Yale University, 1988.

[43] E. Rondio *et al.*, private communication, talk at the Spin Muon Collaboration Meeting, CERN, 2nd March 1995.
[44] EMC, M. Arneodo *et al.*, Nucl. Phys. **B321** (1989) 541.
[45] L. Trentadue and G. Veneziano, Phys. Lett. **B323** (1994) 201.
[46] EMC, M. Arneodo *et al.*, Z. Phys. **C34** (1987) 283.
[47] S. Willocq *et al.*, Z. Phys. **C53** (1992) 207.
[48] J.T. Jones *et al.*, Z. Phys. **C28** (1987) 23.
[49] D. Allasia *et al.*, Nucl. Phys. **B224** (1983) 1.
[50] V. Ammosov *et al.*, Nucl. Phys. **B162** (1980) 208.
[51] J. Ellis, M. Karliner, D.E. Kharzeev, and M.G. Sapozhnikov, *preprint* CERN/TH 94-7326, hep-ph/9412334;
M. Alberg, J. Ellis, and D.E. Kharzeev, *preprint* CERN/TH 95-47; DOE/ER/40427-04-N95, hep-ph/9503333.
[52] The ASTERIX Collaboration, J. Reifenrother *et al.*, Phys. Lett. **B267** (1991) 299;
The Crystal Barrel Collaboration, M.A. Faessler *et al.*, Phys. At. Nuc. **57** (1994) 1693;
The OBELIX Collaboration, V.G. Ableev *et al.*, Phys. At. Nuc. **57** (1994) 1716; Phys. Lett. **B334** (1994) 237;
The JETSET Collaboration, L. Bertolotto *et al.*, Nucl. Phys. **A558** (1993) 27c.
[53] The PS185 Collaboration, P. Barnes *et al.*, Nucl. Phys. **A526** (1991) 575; Phys. Lett. **B229** (1989) 432; Phys. Lett. **B189** (1987) 249.
[54] A. Anselm, M. Anselmino, F. Murgia, and M.G. Ryskin, *preprint* DFTT 48/93.
[55] K. Chen, G.R. Goldstein, R.L. Jaffe and X. Ji, *preprint* MIT-CTP:2365 (1994).
[56] I.I.Y. Bigi, Nuovo Cim. **41A** (1977) 43; Nuovo Cim. **41A** (1077) 581.
[57] G. Gustafson and J. Häkkinen, Phys. Lett. **B303** (1993) 350.
[58] G. Ingelman, proc. *Physics at HERA*, Hamburg, Oct. 29–30, 1991, eds. W. Buchmüller and G. Ingelman.
[59] B. Adeva, A. Gallas, F. Gómez, and C. A. Pérez, *A two-dipole muon DIS spectrometer as* $\Lambda/\overline{\Lambda}$ *polarimeter*, internal note, 1995.
[60] R. Armenteros and J. Podolanski, Phil. Mag. **45** (1954) 13.
[61] A. Kotzinian and C.A. Pérez, $\Lambda/\overline{\Lambda}$ *polarization in SIDIS of polarized muons*, internal note, 1995.
[62] R.L. Jaffe and X. Ji, Phys. Rev. Lett. **67** (1991) 552; Nucl. Phys. **B375** (1992) 527.
[63] The HELP Collaboration, *A proposal for an Internal Jet-Target Experiment at LEP*, CERN/LEPC 93-14, LEPC/P7; CERN/LEPC 94-1, LEPC/P7 Add. 1.
[64] X. Artru, in *Proceeding of the Polarized Collider Workshop*, University Park, Eds. J. Collins, S.F. Heppelman, R.W. Robinett, **AIP 223**, 176 (1990)
[65] X. Artru and M. Mekhfi, Nucl. Phys. **A532** (1991) 351c.
[66] B.L. Ioffe and A. Khodjamirian, *preprint* LMU-01/94 (1994).
[67] F. Baldracchini *et al.*, Fortschritte der Phys. **30** (1982) 505.
[68] X. Artru, J. Czyzewski, and H. Yabuki, *preprint* LYCEN/9423, TPJU 12/94, (1994); X. Artru, private communication.
[69] J. Collins and G.A. Landinski, *preprint* PSU/TH/114 (1994).
[70] A. Kotzinian, *preprint* hep-ph/9412283, *submitted to* to Nucl. Phys. B.
[71] R.D. Tangerman and P.J. Mulders, *preprint* NIKHEF-95-001, hep-ph/9501202.
[72] E.L. Berger, *preprint* ANL-HEP-PR-87-45, (1987).
[73] G. Ross and R. Roberts, *preprint* Ral-90-062, (1990).
[74] S. Peraire, CERN/SL-BT, private communication.

[75] V. Agoritsas *et al.*, CERN/DRDC 91-8, DRDC/P25; CERN/DRDC 93-47.
[76] W. Flegel, CERN/PPE-EC, private communication.
[77] HERA-B proposal, DESY-PRC 94/2, Hamburg, May 1994; LHB Letter of Intent, CERN/LHCC 93-45.
[78] The CsI-RICH Collaboration, A. di Mauro *et al.*, R.D-26 Status Report, CERN/DRDC 94-49, Dec. 1994.
[79] V. Kryshkin *et al.*, *preprint* IHEP 92-95, Protvino;
A. Inyakin *et al.*, CERN/ALICE 93-26, July, 1993;
A. Dolgopolov *et al.*, CERN/ALICE 94-09, May, 1994.
[80] L.L. Frankfurt *et al.*, Phys. Lett. **B230** (1989) 141.